SANDIA REPORT

SAND2004-5397
Unlimited Release
Printed November 2004

Monitoring Stream Stage, Channel Profile, and Aqueous Conductivity with Time Domain Reflectometry (TDR)

Vince Tidwell, James Brainard, Jerome Wright, Amy Coplen, Jesse Roberts, Jason Coombs, and Doug Ruby

Prepared by
Sandia National Laboratories
Albuquerque, New Mexico 87185 and Livermore, California 94550

Sandia is a multiprogram laboratory operated by Sandia Corporation,
a Lockheed Martin Company, for the United States Department of Energy's
National Nuclear Security Administration under Contract DE-AC04-94AL85000.

Issued by Sandia National Laboratories, operated for the United States Department of Energy by Sandia Corporation.

Available to DOE and DOE contractors from
U.S. Department of Energy
Office of Scientific and Technical Information
P.O. Box 62
Oak Ridge, TN 37831

Telephone: (865)576-8401
Facsimile: (865)576-5728
E-Mail: reports@adonis.osti.gov
Online ordering: http://www.doe.gov/bridge

Available to the public from
U.S. Department of Commerce
National Technical Information Service
5285 Port Royal Rd
Springfield, VA 22161

Telephone: (800)553-6847
Facsimile: (703)605-6900
E-Mail: orders@ntis.fedworld.gov
Online order: http://www.ntis.gov/help/ordermethods.asp?loc=7-4-0#online

SAND2004-5397
Unlimited Release
Printed November 2004

Monitoring Stream Stage, Channel Profile, and Aqueous Conductivity with Time Domain Reflectometry (TDR)

Vince Tidwell, James Brainard, Jerome Wright, Amy Copland, Jesse Roberts, Jason Coombs, and Doug Ruby

Sandia National Laboratories
P.O. Box 5800
Albuquerque, New Mexico 87185-0735

Abstract

Time domain reflectometry (TDR) operates by propagating a radar frequency electromagnetic pulse down a transmission line while monitoring the reflected signal. As the electromagnetic pulse propagates along the transmission line, it is subject to impedance by the dielectric properties of the media along the transmission line (e.g., air, water, sediment), reflection at dielectric discontinuities (e.g., air-water or water-sediment interface), and attenuation by electrically conductive materials (e.g., salts, clays). Taken together, these characteristics provide a basis for integrated stream monitoring; specifically, concurrent measurement of stream stage, channel profile and aqueous conductivity. Here, we make novel application of TDR within the context of stream monitoring. Efforts toward this goal followed three critical phases. First, a means of extracting the desired stream parameters from measured TDR traces was required. Analysis was complicated by the fact that interface location and aqueous conductivity vary concurrently and multiple interfaces may be present at any time. For this reason a physically based multisection model employing the S_{11} scatter function and Cole-Cole parameters for dielectric dispersion and loss was developed to analyze acquired TDR traces. Second, we explored the capability of this multisection modeling approach for interpreting TDR data acquired from complex environments, such as encountered in stream monitoring. A series of laboratory tank experiments were performed in which the depth of water, depth of sediment, and conductivity were varied systematically. Comparisons between modeled and independently measured data indicate that TDR measurements can be made with an accuracy of $\pm 3.4 \times 10^{-3}$ m for sensing the location of an air/water or water/sediment interface and ±7.4% of actual for the aqueous conductivity. Third, monitoring stations were sited on the Rio Grande and Paria rivers to evaluate performance of the TDR system under normal field conditions. At the Rio Grande site (near Central Bridge in Albuquerque, New Mexico) continuous monitoring of stream stage and aqueous conductivity was performed for 6 months. Additionally, channel profile measurements were acquired at 7 locations across the river. At the Paria site (near Lee's Ferry, Arizona) stream stage and aqueous conductivity data were collected over a 4-month period. Comparisons drawn between our TDR measurements and USGS gage data indicate that the stream stage is accurate within ±0.88 cm, conductivity is accurate within ±11% of actual, and channel profile measurements agree within ±1.2 cm.

Acknowledgments

The authors want to thank Nancy Hornew and Mike Roark of the U.S. Geological Survey for their assistance and advice in the field-testing of the TDR stream monitoring system. The authors also want to express their appreciation to Timo Heimovaara for his assistance and advice with the multisection modeling. The authors express their appreciation for the assistance of Mike Chapin and Randy Roberts in installing the TDR equipment. Support for this work was derived though Sandia National Laboratories' Laboratory Directed Research and Development Program (LDRD). Sandia is a multiprogram laboratory operated by Sandia Corporation, a Lockheed Martin Company, for the United States Department of Energy's National Nuclear Security Administration under contract DE-AC04-94AL85000.

Table of Contents

1. Introduction

The versatility of time domain reflectometry (TDR) is evidenced by the variety of applications for which this technique has been employed, including locating breaks in long transmission lines [Detlefsen, 1970], monitoring deformation of geologic [Dowding et al., 1989; Kane and Beck, 1996] and engineered materials [Gorski and Anderson, 1998] and for soil moisture sensing [Herkelrath et al., 1991]. These applications take advantage of one or more of TDR's capabilities to 1) locate dielectric discontinuities by tracking arrival times of energy reflections from the resulting impedance mismatches, 2) discriminate the sensitivity of radar energy velocities to different media, and/or 3) measure attenuation of the radar energy in electrically conductive media and solutions. We contend that these same capabilities can be exploited for purposes of insitu stream monitoring. Specifically, TDR has the potential to measure stream stage, channel profile and aqueous conductivity continuously and in real-time.

Admittedly, there are other technologies available for insitu stream monitoring. Float-driven sensors, pressure transducers, and ultrasonic sensors [Latkovitch and Leavesley, 1992] provide accurate measures of stream stage; however, to determine stream discharge from stage requires information on channel profile. Channel profile measurements are still largely measured by hand on a monthly or seasonal basis but other technologies are being developed for continuous monitoring. Fathometers using sonar [Hayes and Drummond, 1995] and radar [Gorin and Haeni, 1989] have been successfully used to bathymetrically determine the channel profile. However, highly turbulent, air-entrained flow conditions, and/or suspended sediment affect instrument readings. Dropping weights and magnetic collar configurations [Richardson and Lagasse, 1994] are relatively inexpensive but have the limitation of not being resettable and susceptibility to binding. Piezoelectric film, mercury tip switches, and magnetic switches mounted on driven rods [Lagasse et al., 1997] provide incremental spatial resolution and the ability to track the entire scour cycle; however, the sensors are delicate and susceptible to damage by ice and debris. An alternative buried device is the neutral buoyancy ball [Zabilansky, 1996], which is equipped with a seismic transducer and radio transmitter that is anchored at varying depths in the channel sediment. As these balls are uncovered and caused to move by the current, their transmitted radio signals are modulated, indicating that the scour has reached their tethered depth. During a depositional event, the balls are reburied, returning to their original depth. While this system can be reset, it's limited to a fairly crude spatial indication of the scour progression. Conductivity is easily measured using electrical conductivity probes, which are sensitive to changes in temperature and the probes are subject to fouling.

The primary advantage of TDR is that with one instrument measurements of stream stage, channel profile and aqueous conductivity can be made continuously and in real-time. Such measurements can be made at as many locations as desired by installing additional probes; for example, along a channel cross-section for channel profiling. Additionally, TDR does not suffer from the limitations noted for the technologies above. However, there are some disadvantages to using TDR in this capacity. First, measurements require probes to be buried directly in the stream channel, thus subjecting them to loss during flood events. Second, complete attenuation of the TDR signal is problematic where the sediments or waters are highly conductive, which could limit application in some environments.

Application of TDR to stream monitoring has been previously explored, primarily in the context of detecting scour around bridge piers. Dowding and Pierce [1994] conducted the first experiments by burying a sacrificial probe in the sediment near a bridge pier. Once a section of the probe was exposed during scouring, the current caused the exposed section to be broken off, shortening the probe and thus changing the TDR signal. Yankielun and Zabilansky [1998] extended this work by conducting proof-of-concept experiments in the lab and field using a fixed probe (i.e., one that would not break off). The field experiments focused on scour near a bridge pier in White River Junction, Vermont with the added complication that the scour was intensified by high-energy flows beneath an ice cover. Based on encouraging results they performed a series of additional laboratory experiments in which they sequentially varied the depth of seven different sediments (sands to cobbles) while collecting accompanying TDR traces [Yankielun and Zabilansky, 1999]. Sediment depths were estimated from the TDR traces by way of the time delay between the negative minima, indicating the sediment/water interface and the positive maxima, indicating the end of the probe. From this approach they found the system capable of measuring changes in sediment depth of less than 5 cm. Using TDR and a variety of other techniques, an extensive survey of river ice influences on channel bathymetry was performed for the Fort Peck reach of the Missouri River [Zabilansky et al., 2002]. Additional field applications of TDR to scour monitoring are given in Zabilansky [2002].

Here, we build on these previous efforts with a focus toward the more general case of stream monitoring. For such application concurrent measurement of stream stage and aqueous conductivity are of interest in addition to the channel scour application described above. More importantly we propose a more robust means of analyzing the TDR data, allowing improved measurement resolution and application to conditions where multiple interfaces exist or multiple parameters are varying simultaneously. The analysis scheme is formulated within a physically based multisection-modeling framework employing the S_{11} scatter function and Cole-Cole parameters for dielectric dispersion and loss. Our objective is to evaluate TDR as an integrated tool for continuous, real-time stream monitoring; specifically, concurrent measurement of stream stage, channel profile, and aqueous conductivity. Efforts toward this goal are organized according to three distinct tasks:

1) Adapt the multisection-modeling framework to the analysis of TDR traces collected within a stream-monitoring context.
2) Perform laboratory experiments to test the multisection-modeling framework and to evaluate the precision and accuracy of the TDR stream monitoring system.
3) Finally, test the TDR stream monitoring system under normal field conditions.

2. Measurement Theory and Multisection Modeling

A typical TDR measurement system consists of a pulse generator, transmission line, and oscilloscope. The pulse generator produces a radar-frequency, fast-rise, step-voltage pulse in the form of an electromagnetic (EM) wave. The EM wave, assumed to be traveling in transverse electromagnetic (TEM) mode, is propagated along the transmission line. The transmission line is generally composed of a length of coaxial cable terminated with a waveguide (Figure 2.1). The waveguide is the "sensor" of the system and is embedded in the medium of interest. The EM wave travels to the end of the waveguide where it is reflected back to the oscilloscope for analysis.

Propagation of the EM wave is dependent on the physical and dielectric properties of the transmission line and the dielectric properties of the medium surrounding the waveguide. In a fluvial environment, a single waveguide could traverse several different media (i.e., air, water, and sediment) each with different dielectric properties such as that depicted in Figure 2.1. Because of the multiple and heterogeneous phases present in fluvial systems, we must look beyond traditional methods [e.g., Topp et al., 1980; Dalton et al.,1984] for analyzing and interpreting the data. Here, we adopt an approach similar to that employed by Heimovaara [1994] and Feng et al. [1999].

With the TDR system, the input signal, $v_o(t)$, and reflected signal or response function, $r(t)$, are measured as a function of time. The response function can be conceptualized as the input function acted upon by the system being tested. This "filtering" of the input signal by the transmission line and sample media is captured in the system function, $s(t)$, and can be represented by the convolution of the input signal with the system function

$$r(t) = \int_{-\infty}^{\infty} v_o(t-\xi)s(\xi)d\xi \tag{2.1}$$

where ξ is an integration variable. The frequency-dependent response function, $R(f)$, can be obtained with the convolution theorem

$$R(f) = V_o(f)S(f) \tag{2.2}$$

in which $R(f)$, $V_o(f)$, and $S(f)$ are the Fourier transforms of $r(t)$, $v_o(t)$ and $s(t)$, respectively, and f is the frequency.

According to this approach, modeling of the TDR trace, $r(t)$, requires definition of the system function. The system function is formulated by recognizing that the EM wave is subject to reflection, transmission and attenuation as it propagates along the transmission line. Specifically, any discontinuity in the dielectric properties along the transmission line produces a reflected and a transmitted wave. Discontinuities occur at points of connection along the transmission line (i.e., coaxial cable/waveguide interface) and at media interfaces traversed by the waveguide (i.e., air/water, water/sediment). The relation between reflection and transmission can be obtained by multiplication of the incident signal by a reflection coefficient and a

transmission coefficient, respectively. The reflection coefficient, $\rho_k(f)$, and transmission coefficient, $\tau_k(f)$, for the *k*th segment of the transmission line (Figure 2.1) are given by

$$\begin{aligned} \rho_k(f) &= \frac{Z_2(f) - Z_1(f)}{Z_2(f) + Z_1(f)} \qquad |\rho_k(f)| \le 1 \\ \tau_k(f) &= 1 + \rho_k(f) \qquad\qquad |\tau_k(f)| \le 1 \end{aligned} \tag{2.3}$$

where $Z_1(f)$ is the frequency dependent impedance for the section of the transmission line in which the reflected wave propagates and $Z_2(f)$ is the impedance for the section of the transmission line in which the transmitted wave propagates. The frequency dependent impedance is calculated with

$$Z_k(f) = \frac{Z_{0k}}{\left[\varepsilon_k^*(f)\right]^{1/2}} \tag{2.4}$$

where Z_{0k} is the characteristic impedance and $\varepsilon_k^*(f)$ is the complex frequency dependent dielectric permittivity of the *k*th segment. Although several models are available for quantifying $\varepsilon_k^*(f)$ of a sample, we adopt the extended Debye relaxation model [Hasted, 1973]

$$\varepsilon_k^*(f) = \varepsilon_{k\infty} + \frac{\varepsilon_{ks} - \varepsilon_{k\infty}}{1 + (i\,f / f_{rel})} - i\frac{\sigma_k}{2\pi f \varepsilon_o} \tag{2.5}$$

where ε_o is the dielectric permittivity of free space (8.854×10^{-12} F/m), i is $\sqrt{-1}$, σ_k the DC conductivity, $\varepsilon_{\infty k}$ the relative high frequency permittivity, ε_{sk} the relative static permittivity, and f_{rel} the relaxation frequency of the *k*th segment of the transmission line. f_{rel} is defined as the frequency at which the permittivity equals $(\varepsilon_s - \varepsilon_\infty)/2$.

Attenuation of the EM wave results from dielectric relaxation and direct current conductivity (e.g., salts or suspended clays). Assuming TEM mode propagation, wave attenuation is given by

$$\gamma_k(f) L_k = \frac{i 2\pi f \left[\varepsilon_k^*(f)\right]^{1/2}}{c} \tag{2.6}$$

where $\gamma_k(f)$ is the complex frequency dependent propagation parameter, L_k is the length of the *k*th section of the transmission line, and c is the electromagnetic wave velocity in a vacuum (3×10^8 m/s).

The system function can be described by way of the $S_{11}(f)$ reflection scatter function [e.g., Clarkson et al., 1977; Heimovaara, 1994; Feng et al., 1999].

$$S_{11}^{k}(f)=\frac{\rho_k(f)+S_{11}^{k-1}(f)\exp(-2\gamma_k L_k)}{1+\rho_k(f)S_{11}^{k-1}(f)\exp(-2\gamma_k L_k)} \tag{2.7}$$

The reflection scatter function is constructed by considering the reflection/transmission that occurs at each dielectric interface along the transmission line and the associated losses. The scatter function is developed in a bottom-up manner starting with the segment most distant from

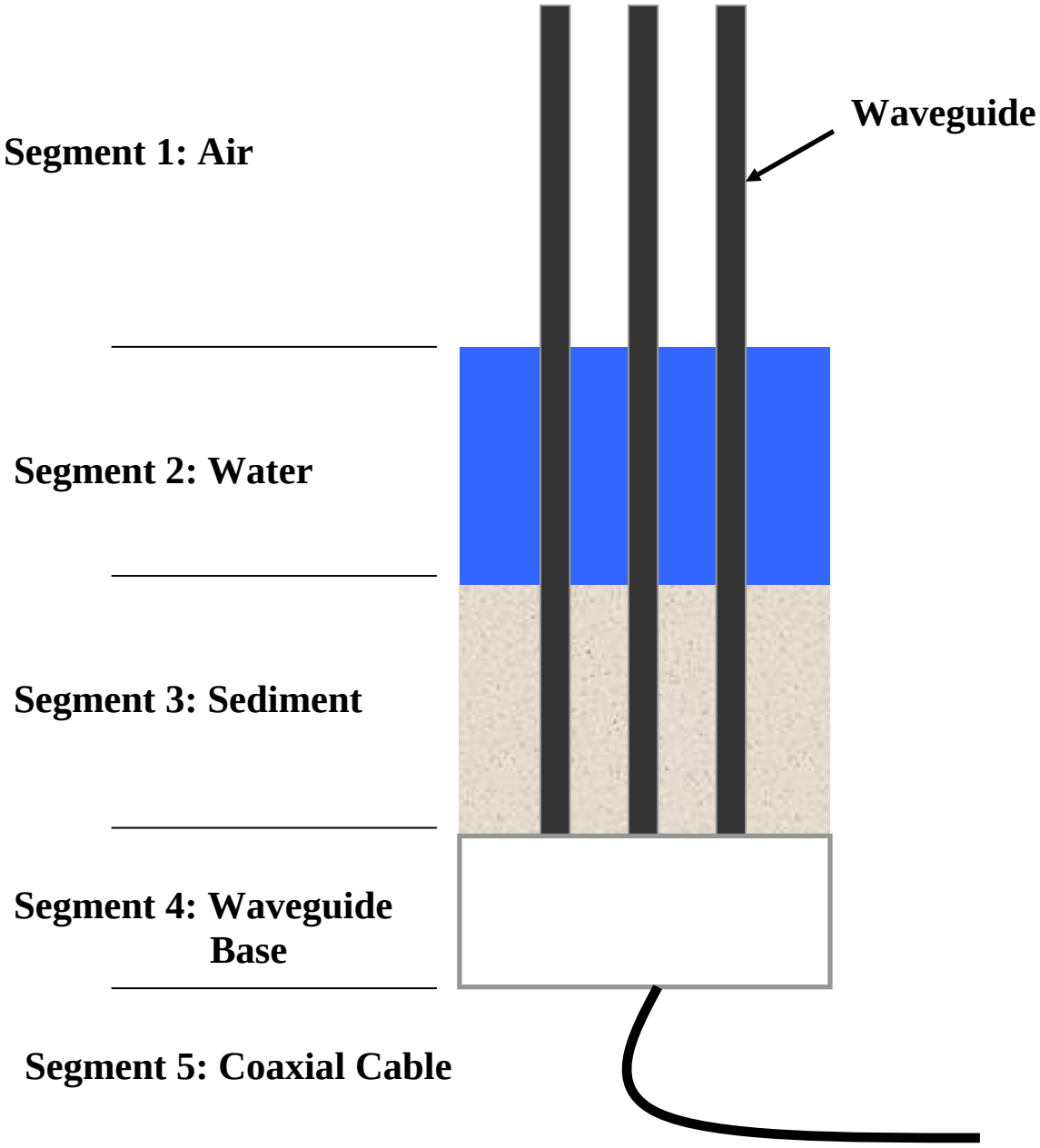

Figure 2.1: Schematic of TDR probe in a fluvial environment. Segment numbers denote sequence for calculation of the multisection S_{11} scatter function.

the cable tester (i.e., segment 1 in Figure 2.1). To start however, an assumption concerning the reflection at the end of the waveguide is required. For a transmission line that is open ended $S_{11}^{0}(f) = 1$, shorted $S_{11}^{0}(f) = -1$ and matched $S_{11}^{0}(f) = 0$. The scatter function for the *k*th segment is calculated from the scatter function for the (*k-1*) section and the reflection coefficient and loss factor for the kth segment. This process is followed until the final segment of the transmission line is reached [see Feng et al., 1999].

3. Laboratory Studies

To evaluate the multisection-modeling process and to determine the accuracy and precision of the TDR monitoring system, a series of controlled laboratory experiments were performed. In these tests the depth of water, depth of sediment, and conductivity along a TDR probe were varied systematically. Acquired TDR traces were then modeled and the results compared against independent measurements of water/sand depth and conductivity. Tests were also conducted to evaluate the consistency of measurements acquired with different probes and with different lengths of coaxial cable.

3.1. Laboratory Methods

3.1.1. Laboratory-Based TDR System

The TDR system employed in our experiments included a Campbell Scientific TDR100 cable tester and a 50-ohm coaxial cable attached to a 3-pronged waveguide. Two different types of coaxial cable were used. For short lengths (1 m) an RG58 (Alpha Wire Co.) coaxial cable was utilized while for longer lengths (2 to 55 m) a low loss Bury-Flex (Davis RF Co.) cable was used. The 3-pronged waveguides (Figure 2.1) were constructed of 0.8 cm diameter stainless steel rod mounted in a watertight polycarbonate base. Waveguide tines measured 17 cm in length, with 2 cm mounted in the polycarbonate and 15 cm exposed for sensing. Spacing between waveguide tines was 2.5 cm. With this configuration, a complete reflection of the signal at the end of the waveguide is assumed; that is, an ideal open-end condition for measurement.

To maximize the information content of the acquired TDR traces, particular attention was given to the selection of an appropriate sampling frequency and sample length. The sampling frequency was defined by the frequency bandwidth of the TDR system, the generally accepted range of which is 20 kHz to approximately 1.5 GHz [Heimovaara, 1994]. The sample length was set such that steady state is reached by the end of the TDR trace. To meet these criteria, a 2048-point trace with a sampling length of 20m was generally found sufficient. With the velocity of propagation set at 1, this yields a sampling frequency of 15.4 GHz, which is a factor of 10 greater than the TDR bandwidth. For measurements made with the longer cables, sampling was initiated at the TDR probe rather than the beginning of the transmission line. All acquired traces were the average of 10 sequential measurements (as performed internally by the cable tester).

3.1.2. Tank Experiments

Laboratory experiments were conducted to evaluate multisection-model, as well as, the precision and accuracy of the TDR system in measuring the depth of water, depth of sediment and conductivity along the length of a waveguide. Tests were conducted in a 30 cm diameter by 30 cm deep acrylic tank in which multiple waveguides were secured. Tests proceeded by sequentially changing the water depth, sediment depth, and/or conductivity, while recording the resulting TDR traces. For example, Test 1 employed four identical waveguides each with a 1-m long cable. Testing was initiated by establishing a static water level (deionized water) 1 cm

above the waveguide base and collecting a TDR trace with each probe. Additionally, 10 sequential measurements were made with one of the probes for evaluating system precision. Then the water level was increased by 1 cm and the process repeated. This process was continued until the top of the probe was reached (15 cm) resulting in the collection of 60 unique measurements and 150 repeated measurements. Other tests included air/tap water, water/sand, air/water/sand, and water with varying conductivity. Finally, 15 waveguides with differing lengths of cable (2, 3, 5, 7, 9, 11,13, 15, 20, 27, 30, 33, 38, 40 and 55 m) were tested to evaluate the effects of cable length on the accuracy of the TDR measurements. Details concerning each test are given in Table 3.1.

For comparison with the acquired traces, independent measurements of the depth of water, depth of sand and conductivity were made. Water and sand depths were measured by way of a graduated scale fixed to the tank, while conductivity and water temperature measurements were made with a conductivity probe (WTW Cond 340i).

3.1.3. Trace Analysis

The next step in the process involved extracting accurate information on the depth of water, depth of sediment and conductivity from the measured TDR traces. This was accomplished by fitting the multisection model described above to the measured traces. Operationally, these parameters were progressively adjusted until an optimal fit (minimum sum of square error) between the model and trace was found. PEST [Doherty et al., 2000], a public domain software package for nonlinear parameter estimation, was used to automate the optimization process.

To accomplish the multisection modeling, detailed information on the dielectric properties of each transmission line segment was required, including the relative high frequency permittivity $\varepsilon_{\infty k}$, the relative static permittivity ε_{sk}, the relaxation frequency f_{rel} and the characteristic impedance Z_{0k}. In some cases, like water and air, these properties were well documented. In other cases only limited data were available (e.g., polycarbonate, and coaxial cable) or the model was only an idealized representation of the actual system (e.g., our three-pronged waveguide is not a coaxial line). For the later cases, these parameters were determined through calibration to acquired traces unique to the TDR measurement system.

Calibration aimed at defining these uncertain dielectric properties made use of a subset of the data collected from static tank experiments, which involved four traces from each of the six tests performed. Here, the measured depths for water/sand and aqueous conductivity were taken as knows, while the uncertain dielectric properties formed the set of fitting parameters. The calibration process began by establishing estimates for each dielectric property. ε_s and ε_∞ values were estimated from reported ranges in the dielectric constant for saturated sand, the coaxial cables, and polycarbonate. Z_o values for the two coaxial cables were estimated from the relation $Z_o = \frac{60}{\sqrt{\varepsilon_s}} \ln\left(\frac{a}{b}\right)$ where *a* and *b* are the inner and outer diameter of the coaxial cable, respectively. Initial best estimates for all other variables were determined using a trial-and-error procedure involving modeling of the calibration data set with the multisection model. Fine-

Table 3.1: Tank experiment details.

Test	Phases	Comments	Unique Measurements
1	Air/Deionized Water	4 identical waveguides with 1-m cables; water level increased by 1-cm increments	60
2	Air/Tap Water	4 identical waveguides with 1-m cables; water level increased by 1-cm increments	60
3	Water/Saturated Sand	4 identical waveguides with 1-m cables; waveguide submerged in deionized water while sand level was increased by 1-cm increments; 40/20 sieve sand was used	60
4	Air/Water/ Saturated Sand	4 identical waveguides with 1-m cables; measurements made with sand depths of 5 and 10 cm, while water level increased by 1-cm increments from sand surface to top of waveguide; 40/20 sieve sand was used	60
5	Water	Single waveguide with 1 m cable; Conductivity increased from 10 to 1000 µS/cm	11
6	Air/Deionized Water	15 roughly identical waveguides with cable lengths of 2, 3, 5, 7, 9, 11,13, 15, 20, 27, 30, 33, 38, 40 and 55 m; water level increased by 4-cm increments	75

tuning of the uncertain dielectric properties was then pursued by way of a semi-automated calibration procedure using PEST. Three to four of the uncertain dielectric parameters would be used as the fitting parameter set while all others were set to their current best estimate. Several iterations were performed varying the fitted and fixed parameter sets while sequentially updating the best estimate values. The relatively large number of uncertain parameters necessitated this piecewise procedure. The resultant parameters taken both from the literature and determined through calibration are given in Table 3.2.

3.2. Laboratory Results

Below a review of the results from our laboratory studies is provided. We first explore the measured traces and how they change with variations in water/sand depth and conductivity. Also reviewed is the nature of the fit between the measured TDR traces and the multisection model. Finally, we turn our attention to an evaluation of the precision and accuracy of the TDR within the context of stream monitoring.

To assist in this discussion a limited but representative set of TDR traces are plotted. Shown are three TDR traces from Test 1 for an air/water system in which the depth of water varies along the length of a waveguide (Figure 3.1), three traces from Test 3 for a water/sand system in which the depth of sand varies (Figure 3.2), three traces from Test 4 for an air/water/sand system in which the depth of sand is held constant at 5 cm while the depth of water varies (Figure 3.3), and three traces from Test 5 for the single phase water system with

Table 3.2. Multisection model properties

Material	ε_s	ε_∞	f_{rel} **(GHz)**	Z_o
Deionized Water	79.9[1]	4.2[1]	17.4[1]	155[2]
Air	1[1]	1[1]	1[1]	155[2]
Water Saturated Sand	19	3.4	6	155[2]
RG58 Cable	2.39	2.05	0.015	75
Bury-Flex Cable	1.6	1.56	0.02	62
Polycarbonate	2.8	2.8	0.1	185[2]

[1] from Hasted, 1973

[2] 3-pronged waveguide

varying aqueous conductivity (Figure 3.4). In each case the measured trace is denoted with a solid line while the fitted multisection model is given by a dotted line. Note that similar results were obtained for the other probes and measurements not shown.

3.2.1. TDR Trace Behavior

In comparing the traces shown in Figures 3.1-3.4, it is apparent that distinct and unique changes in the traces accompany variations in the depth of water and sediment as well as changes in the aqueous conductivity. It is these changes that we exploit in applying TDR to stream monitoring. As water displaces air along the length of the waveguide a proportional change in the shape of the trace occurs (Figure 3.1); specifically, the signal is increasingly impeded due to the higher dielectric of water relative to air. The signal propagating in water is impeded relative to the same signal in air as expressed by the distinct dip in trace values. The minimum threshold reached by the trace is a function of the dielectric; that is, no dip in the case of air, while trace values dip below –0.4 in the presence of water. It is also evident that the time increment over which the trace remains at or near this threshold is directly proportional to the depth of the water. Displacing saturated sand with water has a similar affect (Figure 3.2). As the saturated sand has a dielectric intermediate between air and water, trace threshold values likewise fall between that for air and water. So as the sand depth increases a distinct shoulder on the lower left portion of the trace forms. In the case of the air/water/sand sequence, we see evidence of both of these effects (Figure 3.3). Increasing conductivity has the very apparent effect of attenuating the signal as evidenced by the reduction in the magnitude of the trace at times as early as $t \quad 1.5x10^{-8}$ sec (Figure 3.4).

3.2.2. Comparing Measured and Modeled Traces

Over 300 TDR traces were analyzed with the multisection model. The model was fitted to the data, in a minimum sum of square error sense, by way of the non-linear parameter estimation code PEST. Each trace was modeled using a consistent set of system parameters (see Table 3.2), while the depth of water and sand, as well as the aqueous conductivity were treated as the fitting parameters. Figures 3.1-3.4 provide a visual comparison between the measured data (solid lines) and fitted model (dotted lines) for a limited but representative set of results.

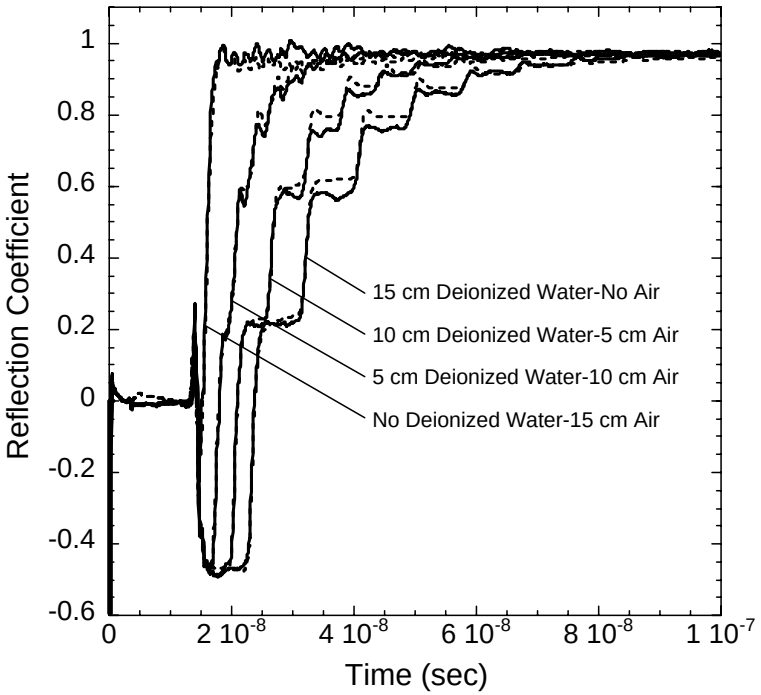

Figure 3.1. TDR traces measured with a varying depth of deionized water along the length of the probe. Shown are traces for water depths of 0, 5, 10, and 15 cm. The solid lines designate the measured traces while the dotted lines correspond to the modeled traces.

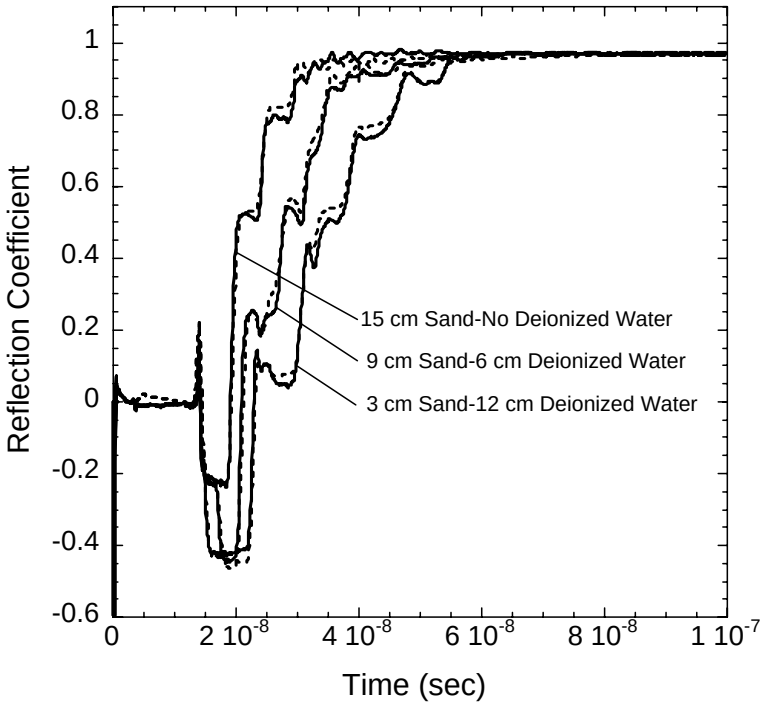

Figure 3.2. TDR traces measured in a layered sequence of sand and deionized water. Shown are traces for a probe submerged in water with accompanying water saturated sand depths of 3, 9, and 15 cm. The solid lines designate the measured traces while the dotted lines correspond to the modeled traces.

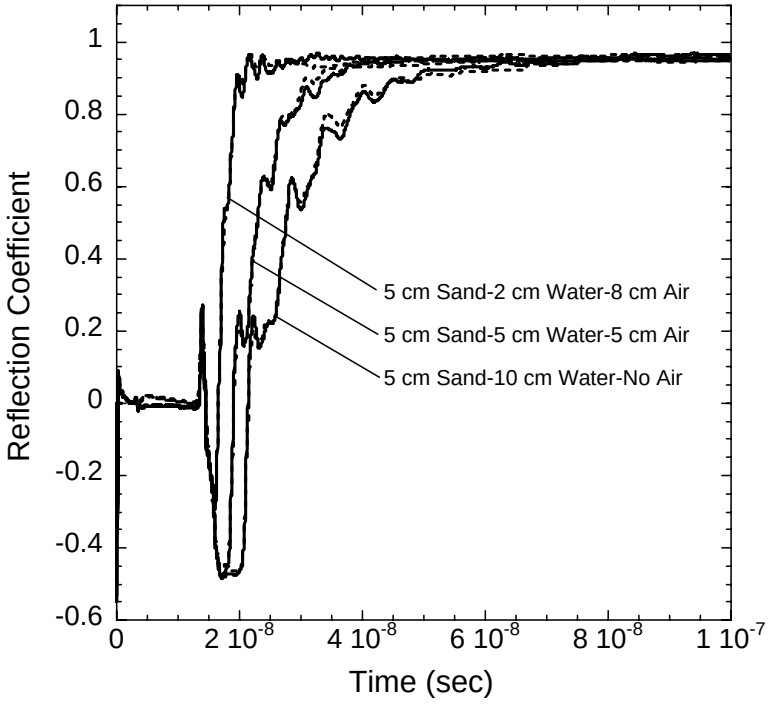

Figure 3.3. TDR traces measured in a layered sequence of sand, deionized water, and air. Shown are traces for a 5 cm depth of saturated sand and increasing depth of water. The solid lines designate the measured traces while the dotted lines correspond to the modeled traces.

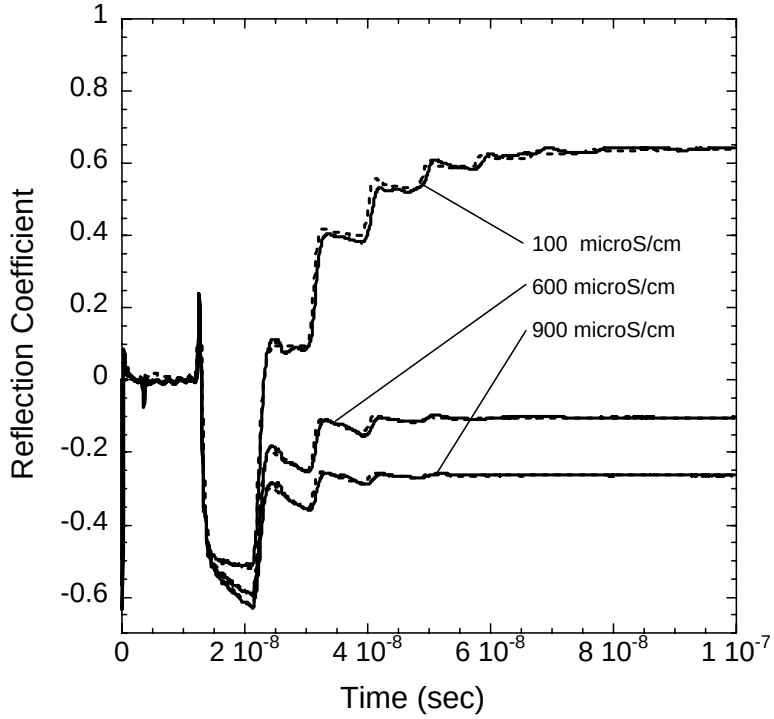

Figure 3.4. TDR traces measured with varying conductivity. Shown are traces for conductivities of 100, 600, and 900 µS/cm. The solid lines designate the measured traces while the dotted lines correspond to the modeled traces.

Inspection of the results shows a generally good fit between the measured traces and the fitted model. Quantitatively, the least square error between the data and model averaged 1.25 and always fell within the limits of 0.11 and 4.45. Although measurements span a broad range of test conditions (different phases, depths, conductivities, and cable lengths) the goodness of fit remained surprisingly stable. That is the same degree of fit was achieved regardless of the test conditions.

Nevertheless there are visible differences in each of the measured/modeled pairs. In particular, there are two sets of errors common to all measured/modeled pairs, one at early times ($t=0.5\text{-}1x10^{-8}$ sec) and the other is evident in the secondary reflections at intermediate times ($t=3\text{-}5x10^{-8}$ sec). In both cases the model consistently over predicts relative to the measured traces; however, the magnitude of the disparity varies between measured/modeled pairs. There are two possible causes. First, these errors may simply reflect inadequate calibration of the model. Given the number of uncertain dielectric properties and the lack of a fully automated calibration procedure, this is a very possible cause of the disparity. In fact, the next phase of this study will consider improved methods for calibration. The second possible cause is that these errors reflect inadequacies in the model to fully capture the effects of the coaxial cable and secondary reflections, respectively, on the TDR signal. However, we must rule out the former before considering the later.

More important than where the measured/modeled traces differed is where the pairs are similar. In all cases the model closely fits the measured data where the trace is rapidly changing; that is, in the falling and rising arms of the trace. This is the case in both the primary and secondary reflections. A close fit between the measured and modeled traces is also consistently achieved at later times ($t>8x10^{-8}$ sec).

It is fortuitous that the model fits the measured traces where it does. It is the steeply falling and rising arms of the trace that marked the points of reflection of the TDR signal, which in turn correspond to the dielectric interfaces of interest. More specifically, it is the time increment between these falling/rising arms (both in the primary and secondary reflections) that quantify the location of the dielectric interfaces. Equally important is the fact that the model fits the data well at late times where the greatest information content on the aqueous conductivity lies. For these reasons the model is able to accurately quantify the location of the air/water or water/sediment interface and the aqueous conductivity, as we will soon see, and for the same reasons the aforementioned errors do not appear to be significant relative to our purposes.

3.2.3. Measurement Precision and Accuracy

Information on the measurement conditions were extracted from each fitted model; specifically, the depth of water and sand along the waveguide as well as the aqueous conductivity. These parameter values were then used along with the independently measured parameter values (i.e., graduated scale and conductivity probe) to assess the precision and accuracy of the TDR measurement system in the context of stream monitoring.

Measurement precision was determined by analyzing the sets of 10 repeated measurements collected with a single probe in Tests 1-4 (see Table 3.1). These sets of data span

the full range of test conditions in terms of depth of air, water and sand as well as a range of different conductivities. Inspection of the results indicates that the error among repeated measurements is essentially uniform across the full range of test conditions. On average the error among repeated measurements was found to be $\pm 1.8 \times 10^{-4}$ m for the depth of any given phase along the waveguide and $\pm 9.75 \times 10^{-5}$ µS/cm for the conductivity. Adopting a confidence interval of two standard deviations, the precision of the TDR in measuring the depth of air/water/sand is $\pm 3.6 \times 10^{-4}$ m while conductivity is measured with a precision of $\pm 1.95 \times 10^{-4}$ µS/cm.

Measurement accuracy was determined by comparing the depth of water/sand and conductivity extracted from the fitted model with that measured independently with the graduated scale and conductivity probe. These analyses made use of the full suite of data collected from Tests 1-6 (see Table 3.1). Errors between the measured and modeled parameters for the different tests and probes were then compared.

Figures 3.5a and 3.5b show scatter plots between the independently measured interface depth data (single interface) and that determined from the fitted model. Results indicated that the errors in the measured/modeled interface depth were surprisingly uniform. Specifically, errors were found to be independent of the probe used, the interface type (i.e., air/water, were found to be independent of the probe used, the interface type (i.e., air/water, water/sediment), the length of the coaxial cable (from1-55 m), and the depth of the interface along the length of the probe. Adopting a confidence interval of two standard deviations, the accuracy of the TDR system to measure the depth of a single interface was determined to be $\pm 3.4 \times 10^{-3}$ m. The one exception noted was when the depths of two interfaces were fitted together (Figure 3.5c). In this situation the accuracy in the depth of either interface fell to $\pm 6.4 \times 10^{-3}$ m. The loss of accuracy arises because of the concurrent fitting of two lengths rather than just one.

Accuracy of the conductivity measurements was also found to be independent of the probe, the length of the coaxial cable, and the number of phases present (Figure 3.6). However, errors between the measured and modeled data were noted to increase with increasing conductivity. Using a confidence interval of two standard deviations the accuracy of the conductivity measurements was found to be ±7.4% of actual.

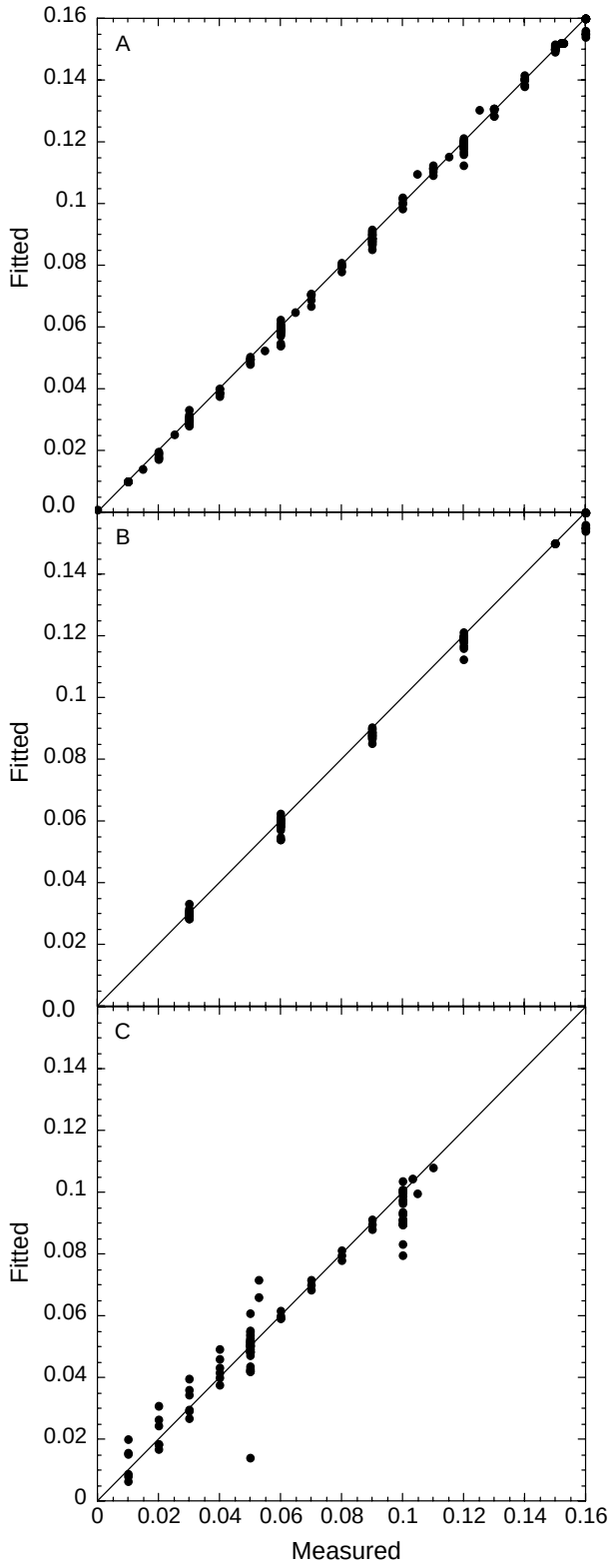

Figure 3.5. Scatter plots showing the difference between the actual interface location and that estimated with the multisection model. A) Scatter plot for all data from Tests 1, 2, and 3; B) scatter plot for all data from Test 6; and C) scatter plot for all data from Test 4. Plotted are the measured/modeled depths of water (m). The line plotted is for the 1:1 relation.

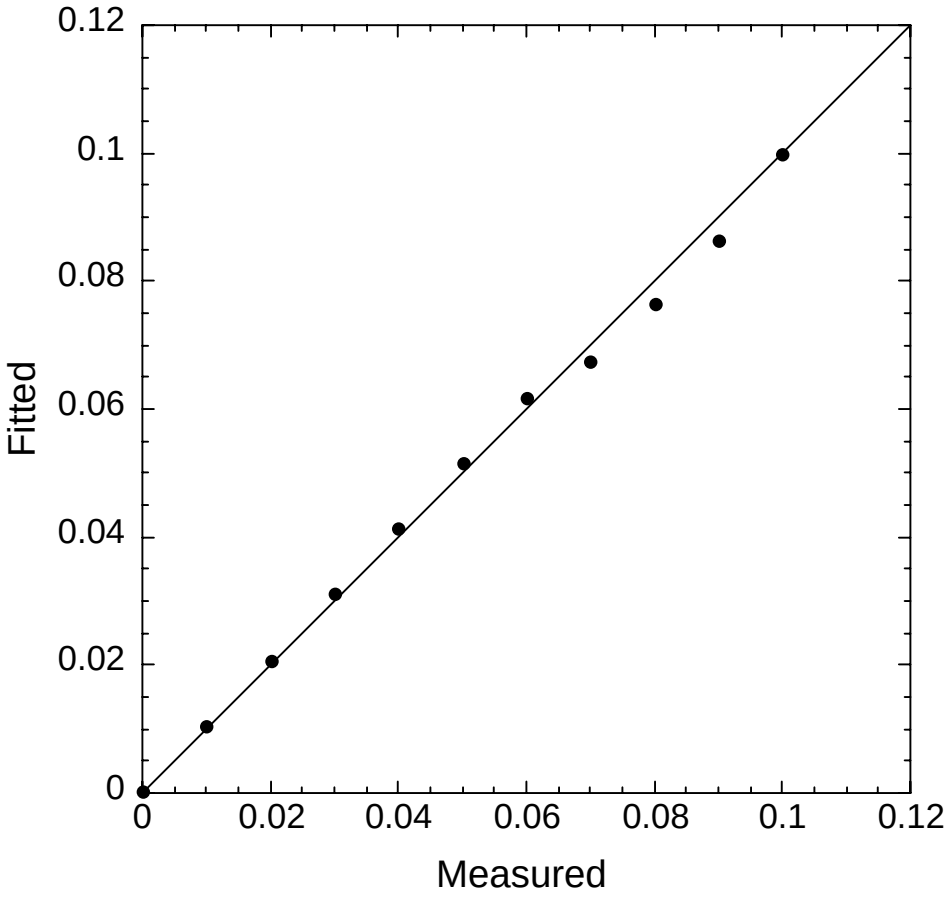

Figure 3.6. Scatter plot showing the difference between the measured aqueous conductivity and that estimated with the multisection model. Data shown are conductivity readings (µS/cm) taken from Test 5. The line plotted is for the 1:1 relation.

4. Rio Grande Study

4.1. Introduction

With headwaters in the San Juan Mountains of southwestern Colorado and flowing south through New Mexico and then along the border between Texas and Mexico, the Rio Grande is an important source of water for much of New Mexico and to a lesser extent, Mexico and Texas. As such, Rio Grande flows are regulated by several dams and monitored throughout its watershed. Within the Albuquerque basin located in central New Mexico, the Rio Grande channel is confined by levees and normally flows within an incised channel except during unusually high flows when the river extends into adjacent levee restricted flood planes. At the lowest flows, the river forms a pseudo-braided streambed.

The objective of a monitoring site on the Rio Grande was to test TDR performance in monitoring streambed dynamics, aqueous conductivity, and stream stage under normal field conditions. The Rio Grande in Albuquerque met several requirements for testing the TDR stream gaging system. First, within Albuquerque, the Rio Grande is rarely dry. A prerequisite for testing the TDR system is having a reliable river to monitor. Second, the river commonly reaches bank-to-bank and at lower flows forms channels around sandbars deposited at higher flows yielding a wide range of conditions under which the TDR system can be tested. Third, a nearby USGS stream gage provides a basis with which to compare TDR stream stage data. In addition to this, the close proximity of the Rio Grande TDR station to SNL allows for frequent visits to take sediment-water and water-air interface measurements. The site chose is just south of the Central Avenue Bridge in Albuquerque.

4.2. Methods

4.2.1. Site Description

To achieve these objectives, seven TDR probes were installed approximately 2 meters apart in a line approximately perpendicular to the riverbank and at an elevation such that the waveguides would not be above the water surface during the lowest expected flows. An eighth probe was installed against the riverbank at an elevation that placed the waveguides within the range of expected water levels. The data acquisition system (DAS) and photovoltaic (PV) equipment were installed on a pole located in close proximity to the bank to allow for short as possible cable runs. A photograph of the site is given in Figure 4.1. Table 4.1 details the TDR DAS equipment and Table 4.2 gives pertinent information on the TDR probes. Photovoltaic equipment details are given in Table 4.3.

TDR data were collected every hour with the DAS along with river temperature and electrical conductivity. The data were uploaded to a computer at SNL through the cell phone. USGS stream flow data were uploaded from the USGS Real Time Stream Flow webpage for comparison with the processed TDR data giving the height of the river surface.

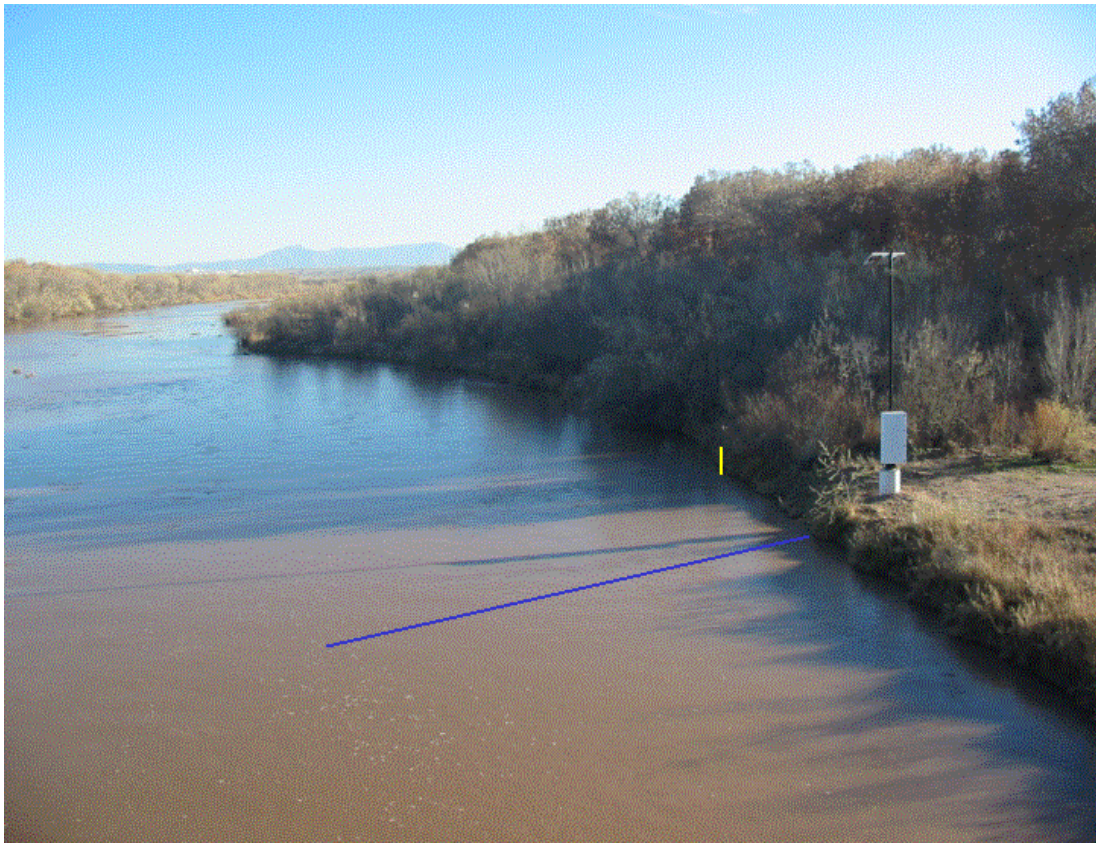

Figure 4.1: View of the Rio Grande TDR station from the Central Avenue Bridge. The Rio Grande TDR station consists of the Data acquisition/PV equipment enclosure mounted to a pole holding the PV panel. The pole is mounted on a 18-inch diameter concrete foundation. The approximate location of TDR probe #1 is indicated by the yellow vertical line downstream and against the right bank while the approximate location of the other 7 probes are indicated by the blue line extending out from the bank.

Additionally, independent sand/water interface measurements were made by hand (see Figure 4.2) for comparison with TDR channel profile measurements. The hand measurement device was constructed out of clear polycarbonate and a meter stick. Hand measuring the sand/water interface involved locating the waveguides with one hand while sliding the grooved base along the waveguide until it hit the riverbed. Once the base was firmly on the riverbed, the slider was moved down the meter stick until it made contact with the top of the waveguide. The device was then removed while holding the slider in the measured position and the distance was read off of the meter stick. TDR measurements were taken before and after the measurement process to evaluate the possibility of erosion of sediment from under the base during the measurement process. At no time during any of the measurements was there any evidence for undermining of the riverbed around the base of the device in that the base stopped at the riverbed surface without any obvious sinking.

4.2.2. Trace Analysis

Analysis of the acquired TDR traces follows the same approach as outlined for the laboratory tests. Specifically, this involved fitting the multisection model to the measured traces to determine the stream stage, channel profile and aqueous conductivity. Operationally, these parameters are progressively adjusted until an optimal fit (minimum sum of square error) between the model and trace is found. PEST [Doherty et al., 2000], a public domain software package for nonlinear parameter estimation, is used to automate the optimization process.

Table 4.1: Rio Grande TDR System Details

Description	Manufacturer/Model	Part Number	Notes
Datalogger	Campbell Scientific	CR10X	1Mb memory expansion
Signal Generator	Campbell Scientific	TDR 100	
Multiplexer	Campbell Scientific	SDMX50	
Coax Cable Connector	RF Industries/ Silver Teflon BNC Male	RF Industries P/N #RFB1101-1SI (Military P/N UG959A/U	
Coax Cable	RF-Davis/BuryFlex	BFLEX	
TDR Probes	Custom Built	None	See Table 4.2 and Figure 4.2
Conductivity/Temperature Sensor	Campbell Scientific	CS547A	
Conductivity/Temperature Sensor Interface	Campbell Scientific	A547	
Enclosure	Campbell Scientific	ENC 16 x 18	Type: NEMA 4X Fiberglass-reinforced polyester Internal Dimensions: 16” x 18” x 9”
Coax Cable Strain Relief	Heyco	PN3231	Liquid tight straight through
Computer/Datalogger Interface	Campbell Scientific	SC532A	Used to download programs to the datalogger
Data Storage Module	Campbell Scientific	AM716	
Cell Phone/Modem	Campbell Scientific	COM-100	
9 pin serial cable	Campbell Scientific	SC12	Provides connection between datalogger and storage module and data logger and computer

To accomplish the multisection modeling, detailed information on the dielectric properties of each transmission line segment is required, including the relative high frequency permittivity $\varepsilon_{\infty k}$, the relative static permittivity ε_{sk}, the relaxation frequency f_{rel} and the characteristic impedance Z_{0k}. In some cases, like water and air, these properties are well documented. In other cases only limited data are available (e.g., polycarbonate, and coaxial cable) or the model is only an idealized representation of the actual system (e.g., our three-pronged waveguide is not a coaxial line). For the later cases, these parameters were determined through calibration to acquired traces unique to the TDR measurement system installed at the test site.

Table 4.2: Rio Grande TDR Probe Specifications

TDR Probe Number	Cable Length (m)	Waveguide Length (m)	Horizontal Distance from Datum (m)	Vertical Distance Between the Top of TDR Block to Datum (m)
1	17.32	0.5	NA	NA
2	7.05	0.16	8.37	2.53
3	9.03	0.16	10.18	2.35
4	10.95	0.16	12.00	2.54
5	13.0	0.16	14.16	2.26
6	15.05	0.16	16.03	2.26
7	17.25	0.16	18.15	2.26
8	19.2	0.16	19.97	2.57

Calibration aimed at defining these uncertain dielectric properties made use of a set of TDR traces collected from the probes following their installation in the river. Here, the measured depths for water/sand and aqueous conductivity were taken as knows, while the uncertain dielectric properties formed the set of fitting parameters. The calibration process began by establishing estimates for each dielectric property. ε_s and ε_∞ values were estimated from reported ranges in the dielectric constant for saturated sand, the coaxial cables, and polycarbonate. Z_o values for the two coaxial cables were estimated from the relation polycarbonate. Z_o values for the two coaxial cables were estimated from the relation $Z_o = \frac{60}{\sqrt{\varepsilon_s}} \ln\left(\frac{a}{b}\right)$ where a and b are the inner and outer diameter of the coaxial cable, respectively. Initial best estimates for all other variables were determined using a trial-and-error procedure involving modeling of the calibration data set with the multisection model. Fine-tuning of the uncertain dielectric properties was then pursued by way of a semi-automated calibration procedure using PEST. Three to four of the uncertain dielectric parameters would be used as the fitting parameter set while all others were set to their current best estimate. Several iterations were performed varying the fitted and fixed parameter sets while sequentially updating the best estimate values. The relatively large number of uncertain parameters necessitated this piecewise procedure. The resultant parameters taken both from the literature and determined through calibration are given in Table 4.4.

Table 4.3: Rio Grande Photovoltaic System

Description	Manufacturer/Model	Part Number	Notes/Specifications
Photovoltaic/TDR Equipment Tower	Custom Built	None	Height: 20 ft Diameter: 6 Inches Type: Schedule 40
75 W PV module	Siemens	BP275	
Pole Mount for PV module	Siemens	DP-SPM1-BP85	
Charge Controller	Mornigstar/SunSaver	SS10L-12	
Battery	Concorde	PVX-490T	2V, 50 Ah AGM battery
Enclosure for Battery, PV Controller, and PV Data Logger	Campbell Scientific	ENC 16X18	Type: NEMA 4X Fiberglass-reinforced polyester Internal Dimensions: 16” x 18” x 9”
PV Datalogger	Campbell Scientific	CR10	For monitoring of PV system performance only
Data Storage Module	Campbell Scientific	SM16	For storing PV performance data only
Surge Arrestor	Delta	LA302	
Load and Charge Current Shunts	Unknown	Unknown	10 A/100mV- Used in conjunction with the datalogger

To facilitate the data analysis process, modeling of the TDR traces was automated. This involved a coupling of the multisection model with PEST. Additionally, pre- and post-processing scripts were developed for inputting the necessary data and for posting and plotting the resulting output. The depth of water on the probe and the aqueous conductivity formed the set of fitting parameters in the trace analysis, subject to the dielectric properties given in Table 4.4. The depth of air or alternatively sand along the probe was determined by subtraction of the fitted water depth from the length of the probe.

Table 4.4. Multisection model properties used at the Rio Grande test site.

Material	ε_s	ε_∞	f_{rel} (GHz)	Z_o
Deionized Water	79.9[1]	4.2[1]	17.4[1]	155[2]
Air	1[1]	1[1]	1[1]	155[2]
Water Saturated Sand	30	3.4	15	155[2]
RG58 Cable	2.39	2.05	0.015	75
Bury-Flex Cable	1.6	1.56	0.02	62
Polycarbonate	2.8	2.8	0.1	185[2]
Mulitplexer	2.1	1.9	2	63

[1] from Hasted, 1973

[2] 3-pronged waveguide

4.3. Results

Operation of the TDR gaging station on the Rio Grande was initiated on March 25, 2004, and has continued to operate to the time of this publication. Measurements are taken every hour at each of the 8 probes installed in the river. One probe is located to monitor stream stage and aqueous conductivity, while the other 7 are positioned to monitor the channel profile (depth of sand on the probe). Below we review the results of this gaging station, drawing comparisons with independently measured data for stream stage, aqueous conductivity, and channel profile.

4.3.1. Instrument Operation

We begin by reviewing the performance of the TDR instrument package, which includes the electronics, waveguides, remote power and telemetry systems. For the most part, the system performed well. Since it began operation, the system has required no special attention; in fact, there have been no lapses in data collection. The designed solar power adequately fueled system operations, while the data analysis and telemetry systems consistently delivered the desired data. However, a few issues have been encountered that deserve attention.

First, and probably most important is the need for longer TDR probes. This need is plainly evident in Figure 4.3 that plots the TDR measured stream stage against that measured by the USGS (see below for more details). Over the 4-months shown in this graph (during high-flow

Figure 4.2: Photograph of the device used to measure sand/water and air/water interfaces relative to the top of the probe

season), the stream-gaging probe was fully submerged on 5 separate occasions, which in one instance lasted for 24 days. That is, anytime the stream stage exceeded 1.09 m the water surface was above the sensing range of the probe. Similar deficiencies were encountered with the probes buried in the stream channel.

Unfortunately, the solution to this problem does not lie simply in extending the length of the waveguides. Making the waveguides longer would increase their susceptibility to damage by debris conveyed downstream by the river and could present a hazard to the public who might recreate in the vicinity of the gaging station. Additionally, lenghtening the waveguides would significantly constrain the range of stream conductivity for which the TDR system could function. That is, the TDR signal is susceptible to complete attenuation at lower aqueous conductivities as the probe length is increased.

To address this issue, preliminary designs have been made and evaluated for a probe with self- adjusting depth. This prototype design calls for a protective probe housing to be buried in the stream channel below the general storm scour depth. The TDR probe, which is affixed to a telescoping rod, is then pneumatically driven from its buried housing. As TDR traces are collected and analyzed, information is fed back to the probe to adjust its position relative to the interface of interest. Current designs specify a probe length of 15 cm that can be adjusted over a 1-meter interval. Costs for a full suite of probes and solar powered pneumatic system is

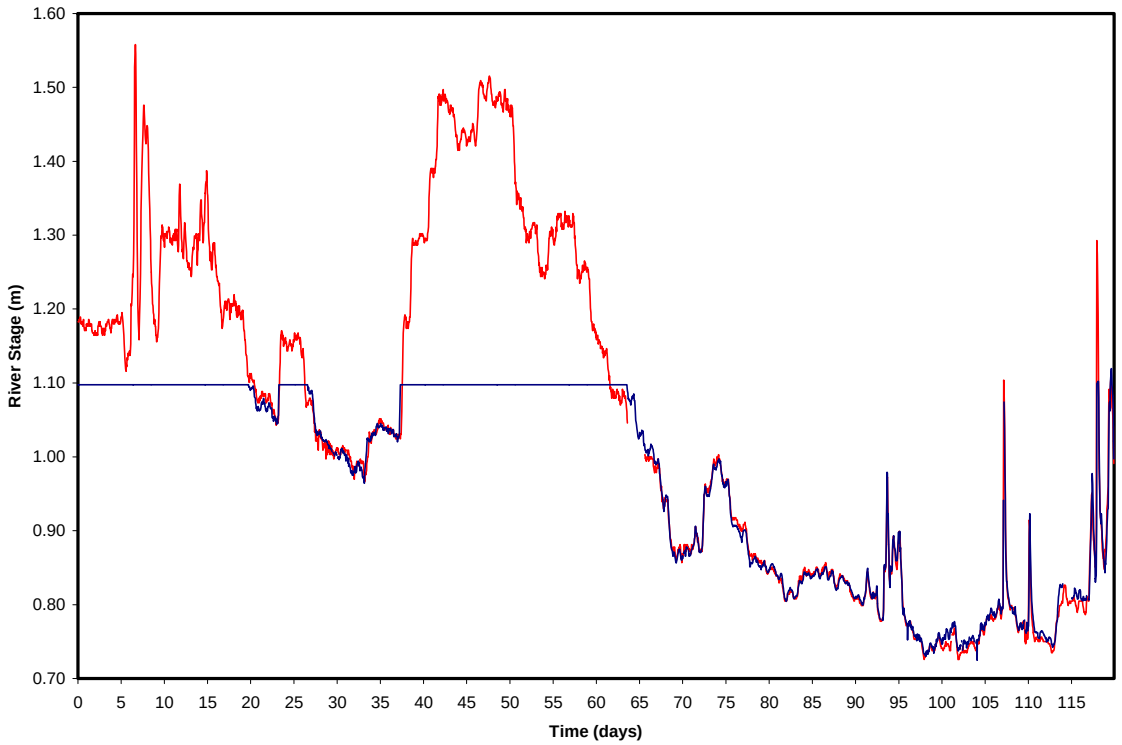

Figure 4.3: Comparison of stage measurements made on the Rio Grande with the TDR (blue line) and as measured by the USGS (red line). Data are for the period of March 25 to July 25, 2004.

competitive with current stream gaging technology. A description and drawing of the prototype probe are given in Appendix A.

The second problem resulted from the process used to install the probes in the river channel. In this case the probes were installed by hand and shovel. As a result, cables connecting two of the probes (probes 5 and 8) to the TDR were inadvertently damaged (cut with a shovel). The result was a loss of useable data from these probes. Greater care will need to be taken with future installations. The probe installation procedures proposed by Zabilansky et al. (2002) involving the use of jetting and surging appear to provide a significant improvement over the hand and shovel approach used here.

The final issue involves the electronics package. Specifically, corrupted TDR traces were periodically recorded by the system. The traces were distorted and shifted to significantly larger values relative to the normal traces. The occurrence of these corrupted traces has yet to be correlated with any distinct external factors. However, it does seem that the distortion is related to the multiplexer or remote power system, as such disparities have never been encountered in the lab. The corrupted traces are not unique to this system as other similar systems deployed in the field have registered similar behavior (e.g., see below for the Paria River). Discussions with the equipment manufacturer have yet to correct or even isolate the problem.

The result of the trace distortion is that viable stream parameters cannot be extracted from the traces. As such, stream stage, conductivity and/or sediment depth measurements are missing for some sampling times. This accounts for a relatively small percentage of the samples; specifically, the percentage of lost data is less than 4% of the total measurements.

4.3.2. Stream stage measurements

For purposes of this analysis, attention will be focused on data collected from June 1 to August 25, 2004. This sequence of time was selected because it provides a period of time in which the river stage rarely deviated above the top of the TDR probed yet still provided an interval in which considerable variations in flow occurred. Measurements of the steam stage are based on the acquire TDR traces from Probe 1 (see Figure 4.1). Examples of some of the acquired TDR traces and the accompanying fitted model traces are given in Figure 4.4. Comparison of the traces reveals a generally good fit between the measured traces and the fitted model. Quantitatively, the least square error between the data and model was always less than 1, and was generally much less than 1. Although measurements span a broad range of test conditions (different stream stage and aqueous conductivity) the goodness of fit remained surprisingly stable. That is the same degree of fit was achieved regardless of the test conditions. Where differences in the measured and modeled traces exist, inadequate calibration of the undocumented dielectric properties (see above) is believed to be the cause.

From the modeled traces fit to the measured data, estimates of the river stage and aqueous conductivity are extracted. These stream stage values are plotted in Figure 4.5. Over this roughly 2-month period the stage of the Rio Grande is seen to vary by over 0.36 m. River stage is seen to follow a general slow decline from July to August reflecting reduced river contributions by melting snowpack. Superimposed on this slow decline are variations occurring on the order of

weeks, which likely reflect deliveries of irrigation water from reservoirs on a tributary to the Rio Grande. Finally, there are some very steep spikes where the stage changed by 30 cm or more in less than a day's time due to local thunderstorms. In each of these cases the TDR monitoring system was able to resolved the variable nature of the river flows as reflected in the changing stream stage.

In efforts to evaluate the accuracy of the TDR to measure stream stage under normal field conditions, comparisons were drawn with stream stage data collected by the USGS. Data were taken from the Rio Grande gage at the Central Bridge in Albuquerque, located approximately 200 m from the TDR site. The vertical offset between the USGS gage and the TDR was calculated by finding the average difference between the USGS and TDR stream stage data. The time series of stream stage data measured by both the USGS and TDR are given in Figure 4.5

Comparison of these two time series reveals a good fit between the TDR and USGS measured stream stage data. In general, the data are in close agreement, rarely deviating by more than 1 cm. An equivalently good fit is realized both with the high intensity, short-time scale events as well as the lower intensity, longer-time scale events. Note that the discrepancy in the two sharp peaks on days 41 and 52 is due to the river stage rising above the top of the TDR probe. Analysis of the error over this approximately two-month period of time establishes that

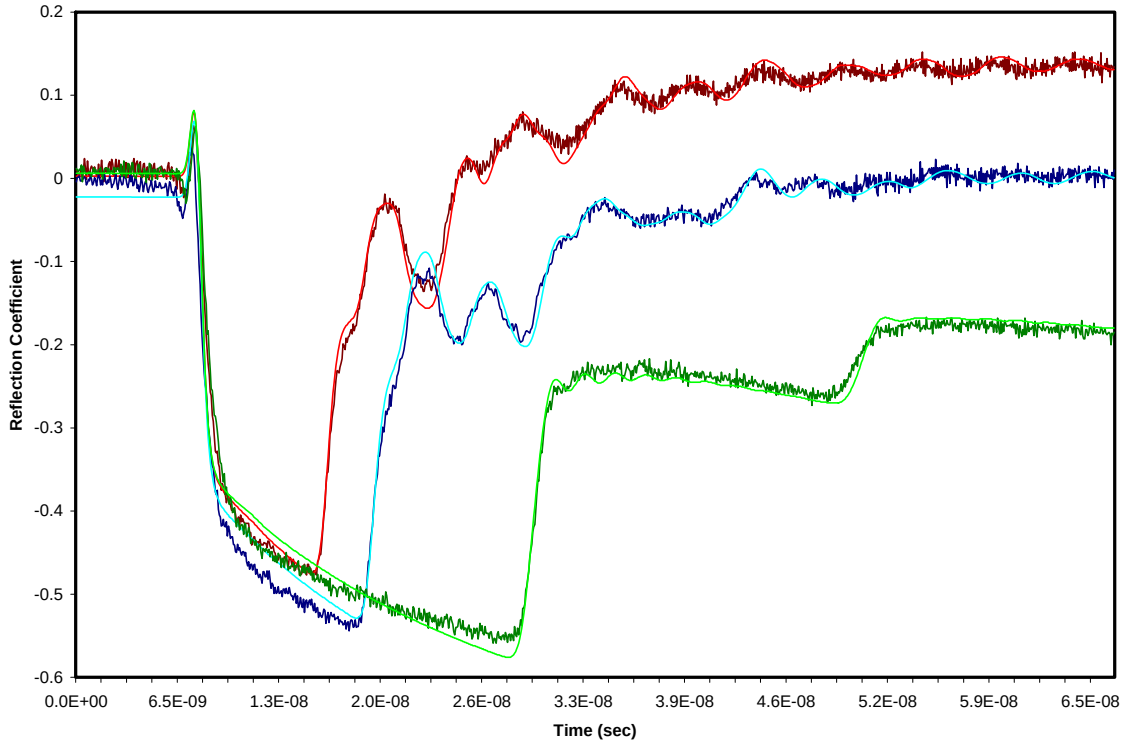

Figure 4.4: Three pairs of measured and modeled TDR traces. The measured trace is always the darker shaded line as well as shows high frequency noise, absent in the modeled traces. As the water depth increases the trace becomes broader and trace values decline at later times.

the TDR measurements are within ±0.88 cm of the USGS measured stream stage values. Considering that the accuracy of the USGS gage is at best ±0.3cm, these results show promise for the TDR stream monitoring system.

4.3.3. Aqueous conductivity measurements

Aqueous conductivity values were estimated from the TDR traces acquired from Probe 1, the same probe used to monitor the Rio Grande's stage. The time series of conductivity data from June1 to July 25, 2004 is plotted in Figure 4.6. The data show a slow rising trend in the conductivity reflecting the slow decline in river discharge. There is one strong spike in conductivity around day 29, the cause of which is uncertain. Conductivity values over this time range from around 0.04 μS/cm to a peak of ~0.1 μS/cm.

To evaluate the accuracy of the TDR measured conductivity values, comparisons were drawn with independently measured conductivity values acquired with a conductivity probe. Conductivity values were measured with a Campbell Scientific Conductivity Probe (see Table 4.1) co-located with Probe 1. Measurements were made every hour, immediately after the acquisition of the eight TDR traces. Measurements from the conductivity probe were adjusted for temperature according to the standard relation

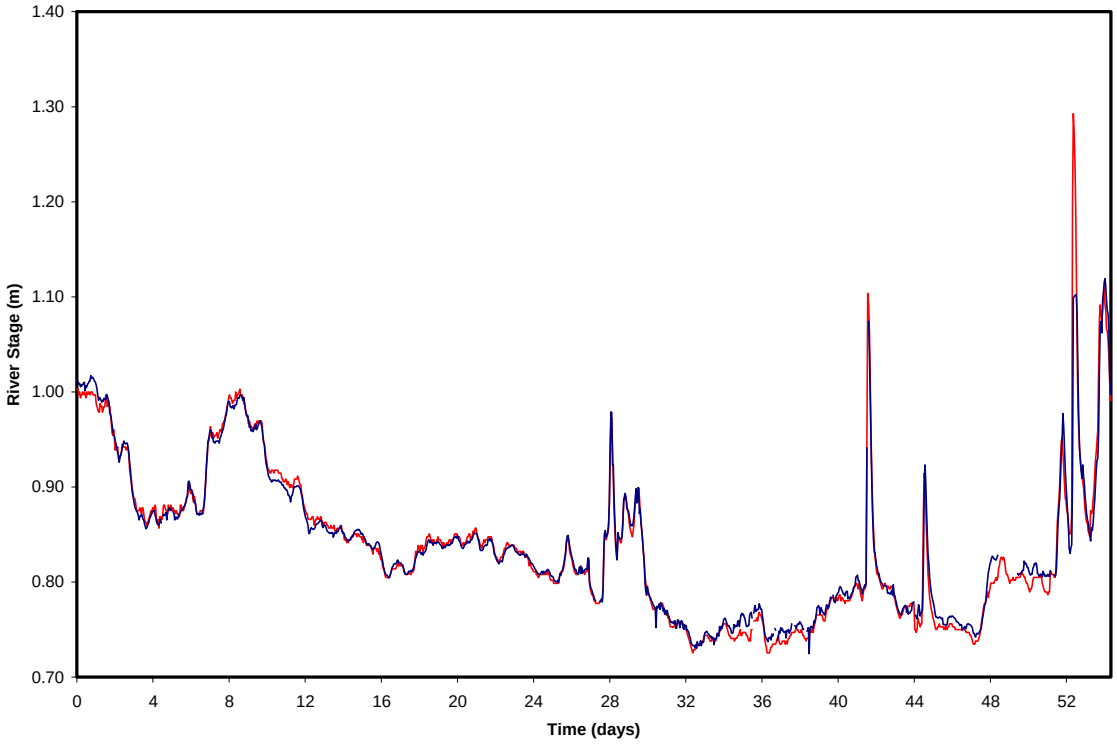

Figure 4.5: Comparison of stage measurements made on the Rio Grande with the TDR (blue line) and as measured by the USGS (red line). Data are for the period of June 1 to July 25, 2004.

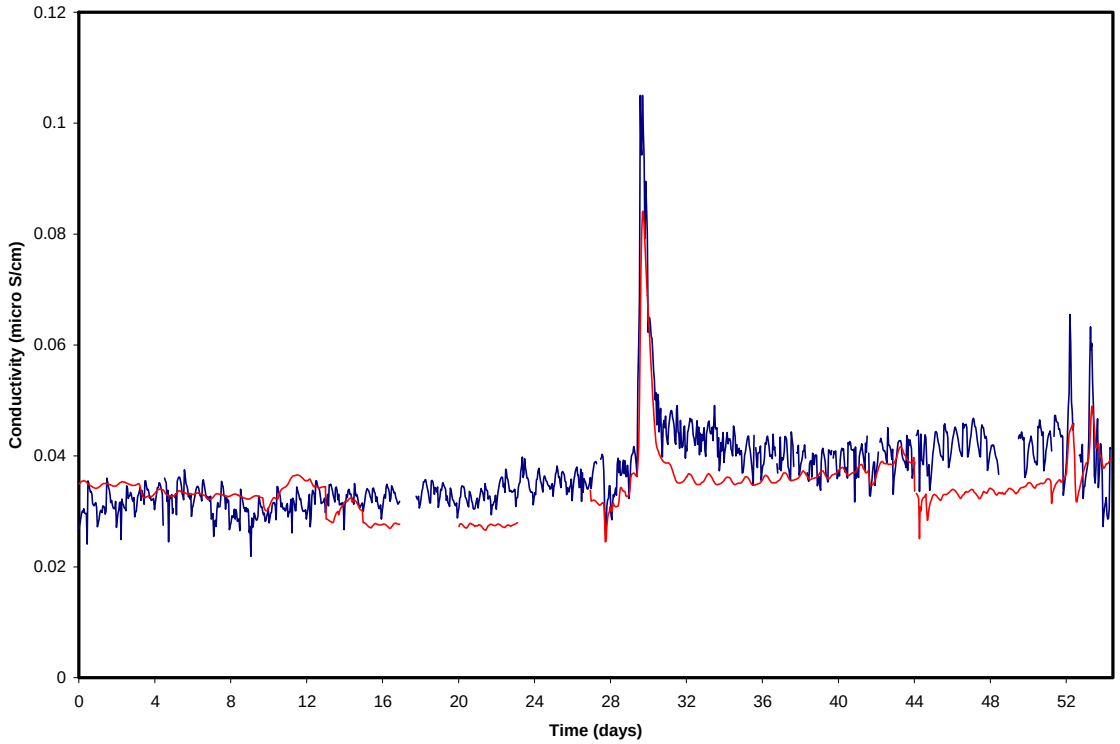

Figure 4.6: Comparison of aqueous conductivity measurements made on the Rio Grande with the TDR (blue line) and conductivity probe (red line). Data are for the period of June 1 to July 25, 2004.

$$\sigma_{25} = \frac{\sigma_o}{(1 - 0.2(25 - T))} \tag{4.1}$$

where T is the temperature in degrees Celsius, σ_o is the measured conductivity and σ_{25} is the conductivity normalized to a temperature of 25 °C. Conductivity data acquired from TDR traces showed no correlation to temperature.

Both the TDR and conductivity probe measured conductivities are shown in Figure 4.6. Both sets of data reflect the slow increase in conductivity and capture the spike at day 29. Further inspection of the data reveal that the TDR measured conductivity is much more noisy than that measured with the conductivity probe. That is, the TDR measured conductivity consistently fluctuated by 0.005 to 0.01 μS/cm over time intervals of 4 to 12 hours. The TDR also tended to overestimate the conductivity during peak events. The average error measured over this roughly two-month period was 0.0046 μS/cm, which is approximately 11% of the average conductivity. This result is consistent, albeit a little higher, than what we found in the laboratory experiments.

4.3.4. River channel measurements

Continuous monitoring of the Rio Grande channel profile was also performed; specifically, measurement of the constant scour and redeposition of sediments. Such monitoring was performed with 7 different probes anchored to the channel bed (see Figure 4.1). The probes were buried to different depths to provide a broad range over which to monitor sediment dynamics. Monitoring involved measuring the depth of sediment on the probe as estimated from the acquired TDR traces. As noted earlier, two of the probes, probes 5 and 8, were damaged upon installation and thus yielded no useful information. Here we review the results for the 5 other probes.

To evaluate the accuracy of these measurements, independent channel profile measurements were made by hand. The hand measurements, as described above, were collected over a six-month period of time resulting in the acquisition of 47 contemporaneous hand-TDR measurements. The corresponding TDR traces were modeled yielding estimates of the sediment depth. A scatter plot of the hand-measured depths verses the TDR measured depths is given in Figure 4.7. From the plot it is apparent that the data are strongly linearly correlated; however, the TDR measurements do tend to slightly overestimate the hand measurements. The average error between the hand and TDR measurements is ±1.25 cm. As it is very difficult to make the hand measurements without some disturbance of the sediment interface, the reported error is considered quite acceptable.

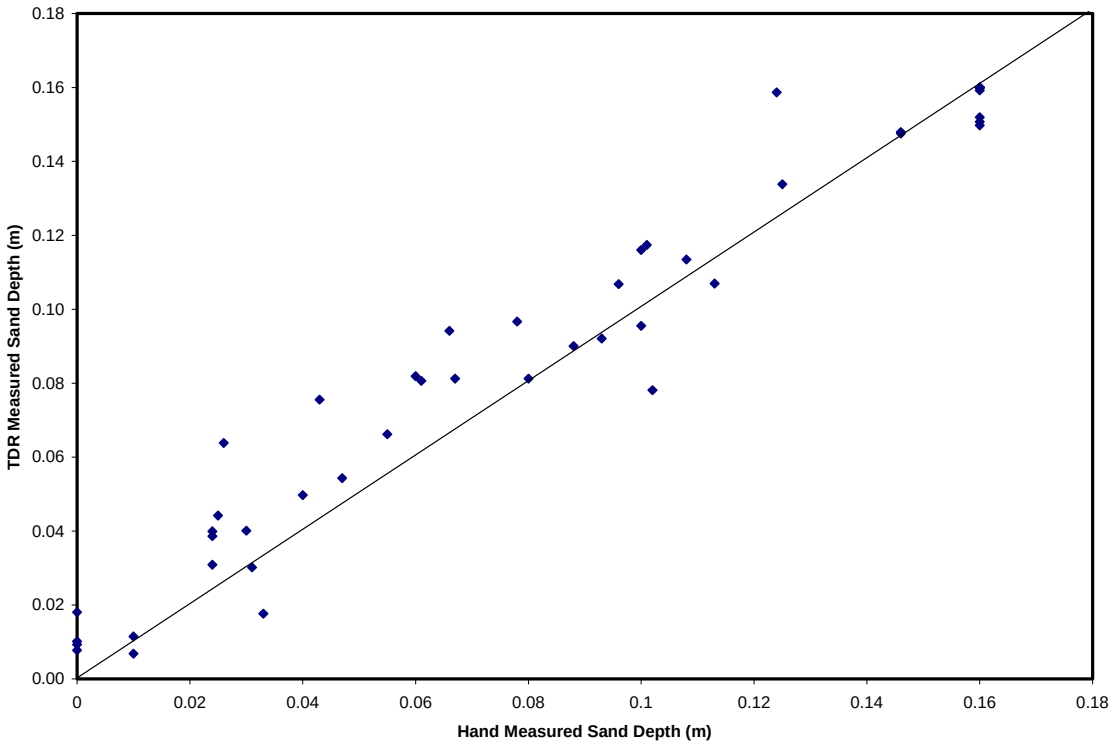

Figure 4.7: Scatter plot between sand depth measurements made by hand (see Figure 4.2) and those estimated from TDR traces. TDR traces were taken from the probes buried in the channel of the Rio Grande.

The depth of sand on the probe verses time is plotted for probes 3, 6, and 7 in Figure 4.8. Data are for the period of June 1 to July 25, 2004, consistent with that considered for the stream stage and aqueous conductivity analyses. Probes 2 and 4 are excluded as they remained buried in sand over this entire period of time (the deepest of the five operational probes). At first glance the three plots appear very noisy where sand depths vary by 5-10 cm in the matter of a few hours. This behavior is evident in all three-time series until about day 40 when the three probes become generally exposed above the channel bottom.

To explore whether this behavior is real or an artifact of the measurement, we reviewed the acquired TDR traces. Specifically, a comparison of the measured and modeled traces was performed (e.g., Figure 4.9). In general, results revealed a good fit; in fact, the least square error between the data and model was consistently below 1. Additionally, this degree of fit was achieved whether the sand depth was near the top or the bottom of the probe. Considering that we are accurately modeling the traces and that our measurement error is low (± 1.25 cm), we conclude that this continuous oscillation in the sand depth is real.

These oscillations reflect the active transport of sand downstream by the Rio Grande. This mobile bedload appears to be composed of three superimposed components. The smallest scale feature corresponds to a continuous string of sand waves. By windowing in on these features (see Figure 4.10), these sand waves are seen to have an amplitude of 7-10 cm and wavelength of 3-4 hours. The next larger feature is a set of sand dunes with an amplitude in excess of 16 cm and a wavelength of roughly 28 days. Finally, the waves and dunes are followed by a mobile sandbar that completely overwhelms the system (complete erosion of the sand bar to a depth below the probes) in the later part of this time series. The presence and mobility of these sand features is further supported by casual observations made during the installation of the TDR equipment and during the collection of the hand-measured channel depths.

These measurements quantifying the mobile bedload phase conveyed within a major river channel are unique. To the knowledge of the authors, no similar measurements have ever been published. These results demonstrate the potential for TDR to track the movement of sand and/or silt sized particles as bedload in an aqueous environment. Such time series as presented here could be used to develop quantitative estimates of the mobile bedload phase by simply integrating the area under the measured sand depth curves. By repeating this at several locations along a channel cross sections the mobile bedload for the entire river could easily be calculated.

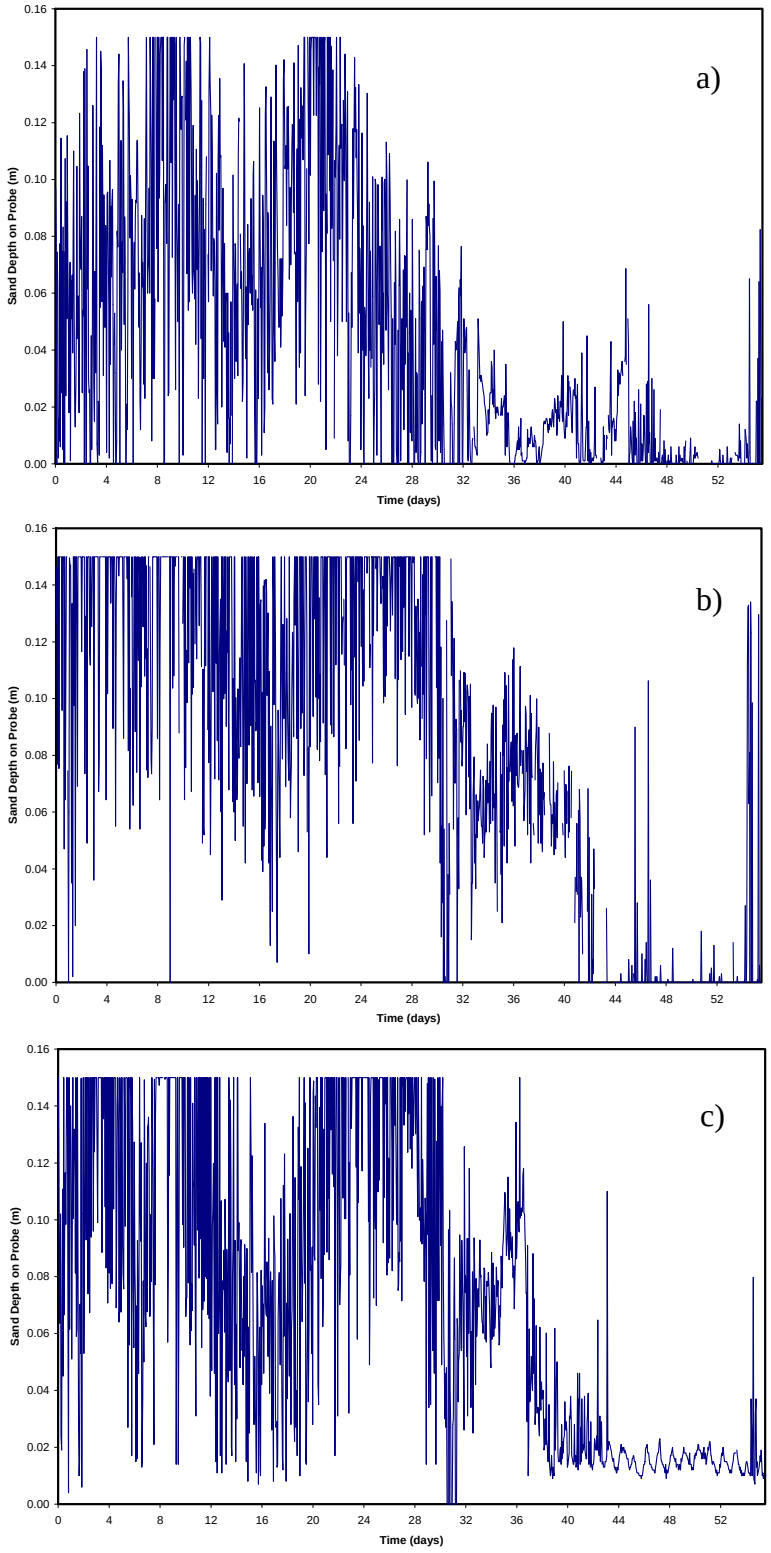

Figure 4.8: Time series of sand depth on TDR probes buried in the channel of the Rio Grande. Variations in sand depths reflect movement of sand waves, dunes, and bars across the probes. Data are for probes a) 3, b) 6, and c)7.

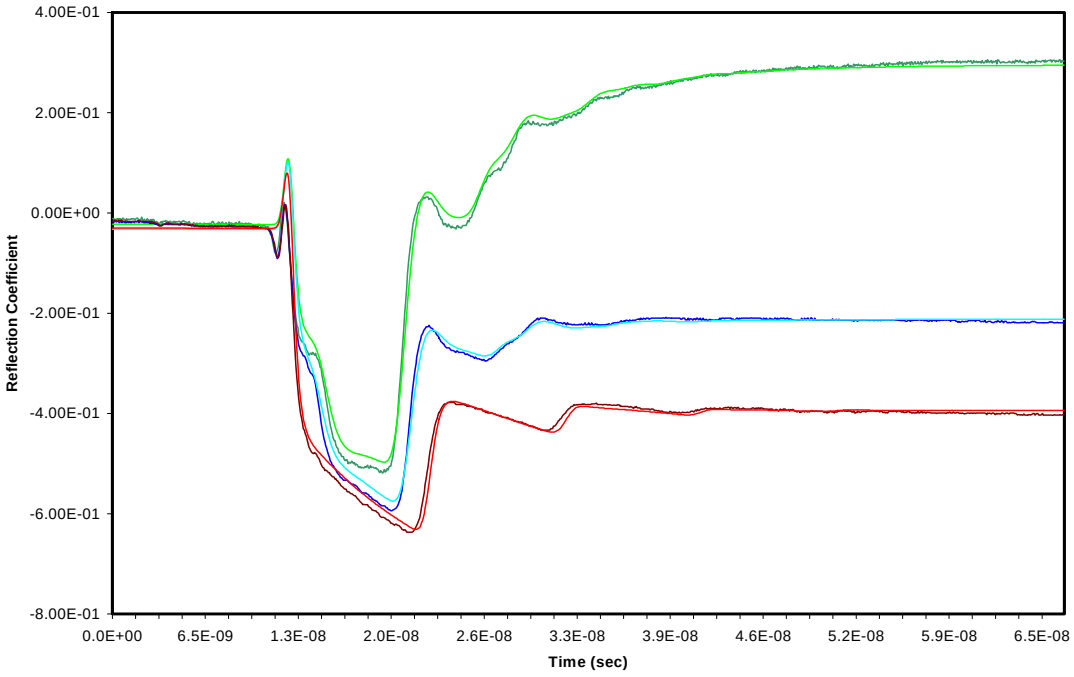

Figure 4.9: Three pairs of measured and modeled TDR traces. The measured trace is always the darker shaded line as well as shows high frequency noise absent in the modeled traces. Trace narrows as sand replaces water along the probe.

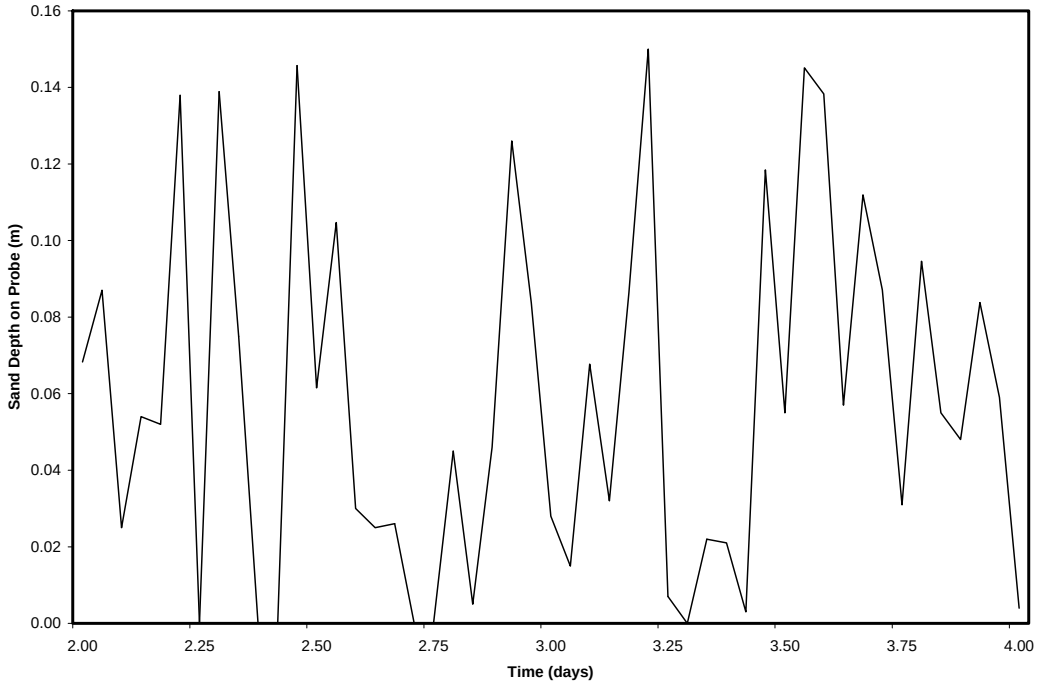

Figure 4.10: Time series of sand depth measurements made with Probe 3 over a 2-day period (focused view of days 2 and 3 shown in Figure 4.8a).

5. Paria River Study

5.1. Introduction

The Paria River is a major tributary to the Colorado River in Northern Arizona where it enters the Colorado River at Lee's Ferry, 13 miles down stream from Glen Canyon Dam. Its head waters are to the north of the Colorado River within the foothills of the Paunsaugunt Plateau, a major dissected plateau in southwestern Utah ranging to elevations of 9300 ft. The river is 75 miles long with its upper part flowing generally through open valleys with gently sloping sides and the lower part flowing through a slot canyon with sheer walls approaching 1000 feet and in places only ten feet apart. Flows in the Paria near its mouth are usually less than 10 cubic feet per second but exceed 10000 cubic feet per second during intense monsoon storms during which times millions of metric tons of sediments are transported to the sediment starved Colorado River. In addition some reaches of the Paria exceed EPA limits of salinity, chloride and total dissolved solids. Because of these factors alone, discharge and water quality measurements play a central role in several management arenas of the Colorado River below Glen Canyon Dam.

In contrast to the Rio Grande stream-monitoring project, the objective of the Paria River project was to test the ability of TDR to capture both the rise and fall of high discharge events while continuously monitoring salinity. The site was chosen because of problems that the USGS station encounters during waning floods when sedimentation within the float chamber prevents accurate stream flow measurements.

5.1. Methods

5.1.1. Description of Site

The TDR monitoring system was mounted immediately next to the USGS station and used the station structure as support for the TDR probes which were stacked vertically to capture a wide range of flows (Figure 5.1 and 5.2). The probes were arranged with shorter waveguides on the bottom of the stack and longer waveguides upwards with the top of the lower waveguides level with the bottom of the waveguide of the higher probe. With the exception of the mounting hardware, waveguide lengths, and cable lengths, the TDR probes were of the same construction of the probes used in the Rio Grande Study (Table 4.2). The waveguide and cable lengths are specified in Table 5.1.

The Paria River monitoring station incorporated all of the same equipment installed at the Rio Grande (Table 4.1) except for the cellular phone, modem and PV system. At the Paria, data was uploaded from a storage module (Table 5.2) while a smaller PV system (Table 5.2) provided power. Other differences included cable lengths, waveguide lengths and the installation arrangement of the TDR sensors.

Figure 5.1: View of the USGS gauging station at the Paria. The TDR monitoring system is mounted on the frame work of the USGS station and consists of the white enclosure seen midway up the stilling station above the larger brown enclosure and a stack of TDR probes immediately to the left of the stilling station. See Figure 4.2 for a close-up view of the TDR stack.

5.1.2. Trace Analysis

Analysis of the acquired TDR traces follows exactly the approach adopted for the Rio Grande Site. Details can be found in Section 4.2.3. Modeling involved the fitting of the multisection model to the measured traces to determine the stream stage, and aqueous conductivity. Model fitting was automated through application of the nonlinear parameter estimation package, PEST. Model calibration was necessary to define the undocumented dielectric properties required by the model. Due to the similarity of calibration results, parameters used to model the Paria TDR traces are the same as used for the Rio Grande data (Table 4.4).

5.2. Results

Operation of the TDR gaging station on the Paria River was initiated on May 25, 2004, and was discontinued on October 24, 2004. Measurements were taken at 15-minute intervals for continuous monitoring of river stage and aqueous conductivity. Below we review the results of this gaging station, drawing comparisons with independently measured stream data.

Figure 5.2: Close-up view of the TDR probe stack. Seven probes are visible with the top of the waveguides of the eighth probe barely visible at the water surface.

5.2.1. Instrument Operation

Again, we begin our analysis by considering the performance of the TDR instrument package, which includes the electronics, waveguides, and remote power. Consistent with the Rio Grande site, the system performed well. During its roughly four months of operation, the system required no special attention and no lapses in data collection were encountered. The only real issue involved the electronics package in which corrupted TDR traces were periodically recorded. In fact, the corrupted traces measured at the Paria are very similar to that gathered at the Rio Grande site.

The corrupted traces have a very distinct signature; specifically, the shape of the trace is distorted and the values exhibit a distinct positive shift relative to the normal traces. No external factors could be linked to the behavior, nor could the manufacturer assist with the problem. Unlike the Rio Grande site, all traces showed some degree of corruption. In many cases the corrupted files could be analyzed; however, where the corruption was significant the traces could not be modeled. For these sampling times, stream stage and conductivity values are lacking. These significantly corrupted traces account for a considerable fraction of the data. At the Paria River site, approximately 25% of the data were lost due to trace corruption.

Table 5.1: Rio Grande TDR Probe Specifications

TDR Probe Number	Cable Length (m)	Waveguide Length (m)	Vertical Distance Above Datum (m)
1	8.98	1.0	2.08
2	8.98	0.50	1.58
3	8.96	0.50	1.08
4	8.96	0.30	0.78
5	8.93	0.30	0.48
6	8.98	0.16	0.32
7	8.96	0.16	0.16
8	8.91	0.16	0.0

Table 5.2: Partial list of monitoring equipment used at the Paria River: For a complete list see Table 4.1

Description	Manufacturer/Model	Part Number	Notes
Storage Module	Campbell Scientific	SM16M	Replaced the function of the cell phone used at the Rio Grande Station
Computer-Datalogger Interface	Campbell Scientific	SC532A	Used to download data from the storage module to the computer

Table 5.3: Paria River Photovoltaic System Details

Description	Manufacturer/Model	Part Number	Notes
9.4 Watt PV module	Solarex	MSX10	
24 amp hour battery	Campbell Scientific	BP24	
Charge Controller	Campbell Scientific	CR112R	

5.2.2. Stream stage measurements

Analyses focus on the data collected from May 25 to July 26, 2004, which was the set of available data at the time of this publication. An example of an acquired TDR trace and the accompanying fitted model trace is given in Figure 5.3. From this comparison it is apparent that the degree of fit between the measured and modeled traces is not as good as it was for the Rio Grande. Quantitatively, the least square error between the data and model was generally greater than 2 and sometimes more than 3. Also evident is a positive shift in the data relative to the traces gathered in the lab or from the Rio Grande site (Figure 4.4). Accompanying this positive shift is a slight distortion of the shape of the traces, which is the cause of the degraded fit between model and trace. As noted above, the cause of this distortion is unknown, thus preventing the modeling or correction of this effect.

From the modeled traces fit to the measured data, estimates of the river stage and aqueous conductivity were extracted. The stream stage values are plotted in Figure 5.4. Over this

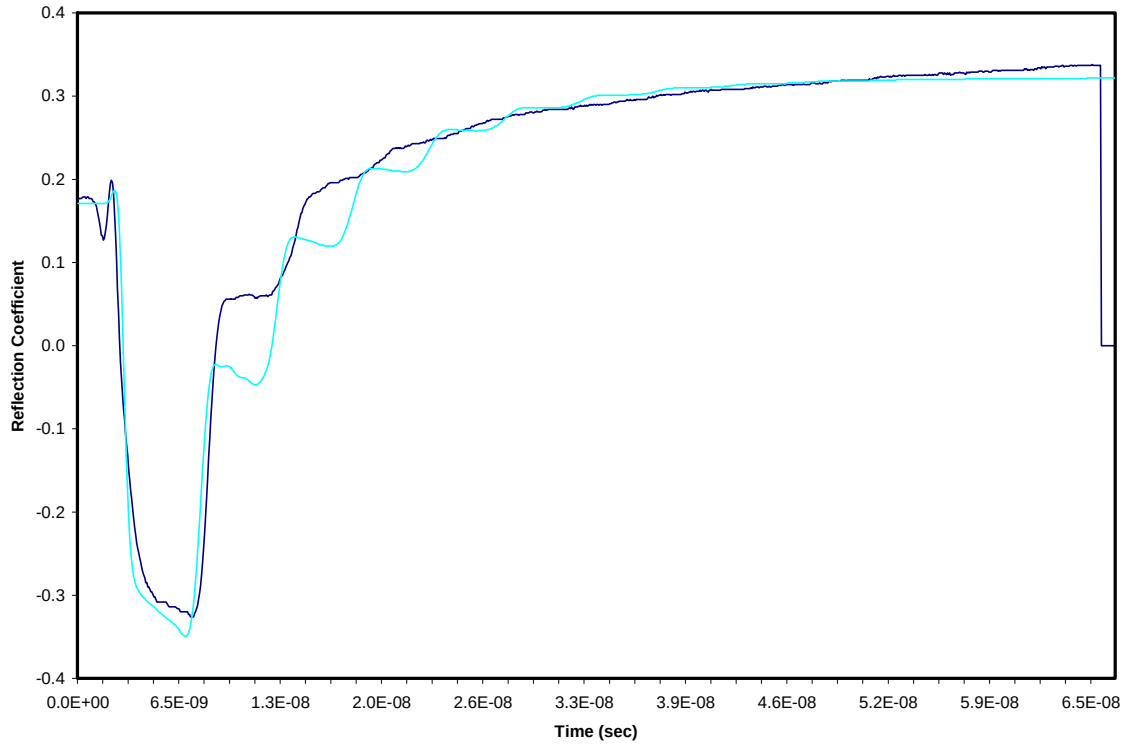

Figure 5.3: A pair of measured and modeled TDR traces. The measured trace is the dark blue line. Notice the trace is initiated at a value of 0.18 as opposed to 0 for the other traces shown.

roughly 2-month period the stage of the Paria River is seen to vary by over 0.56 m. For the first 50 days the river stage is almost constant for this relatively small, unmanaged tributary to the Colorado River. However, over the last 12 days of the record several intense thunderstorms caused rapidly changing flows on the Paria River.

To extend our analysis of the accuracy of the TDR stream monitoring system, comparisons were drawn between the TDR data from the Paria River and stream stage data collected by the USGS. The USGS data were taken directly from the "Paria River at Lees Ferry, AZ" gage that was co-located with the TDR gaging station. The time series of stream stage data measured by both the USGS and TDR are given in Figure 5.4.

For the first 50 days of the analysis the TDR measurements track the USGS stream stage measurements very well. The average difference between the two measurements is only 0.004 cm; however, the stream stage varied by only 2.4 cm over this time. This is not the case for the last 12 days where several distinct flow events occurred and the fit between the TDR and USGS stream stage data deviate significantly. In all but one case (the event from day 55.5 to day 56.3), the TDR was able to accurately detect the onset of the flow event and the duration of the event. However, the TDR did a relatively poor job at measuring the intensity of the events. Specifically, the TDR underestimated the stage for the flash events that occurred on days 50 and 60, and consistently underestimated the recession limb of the hydrograph for the series of events occurring from day 51 to day 53. These discrepancies appear related more to the algorithm used

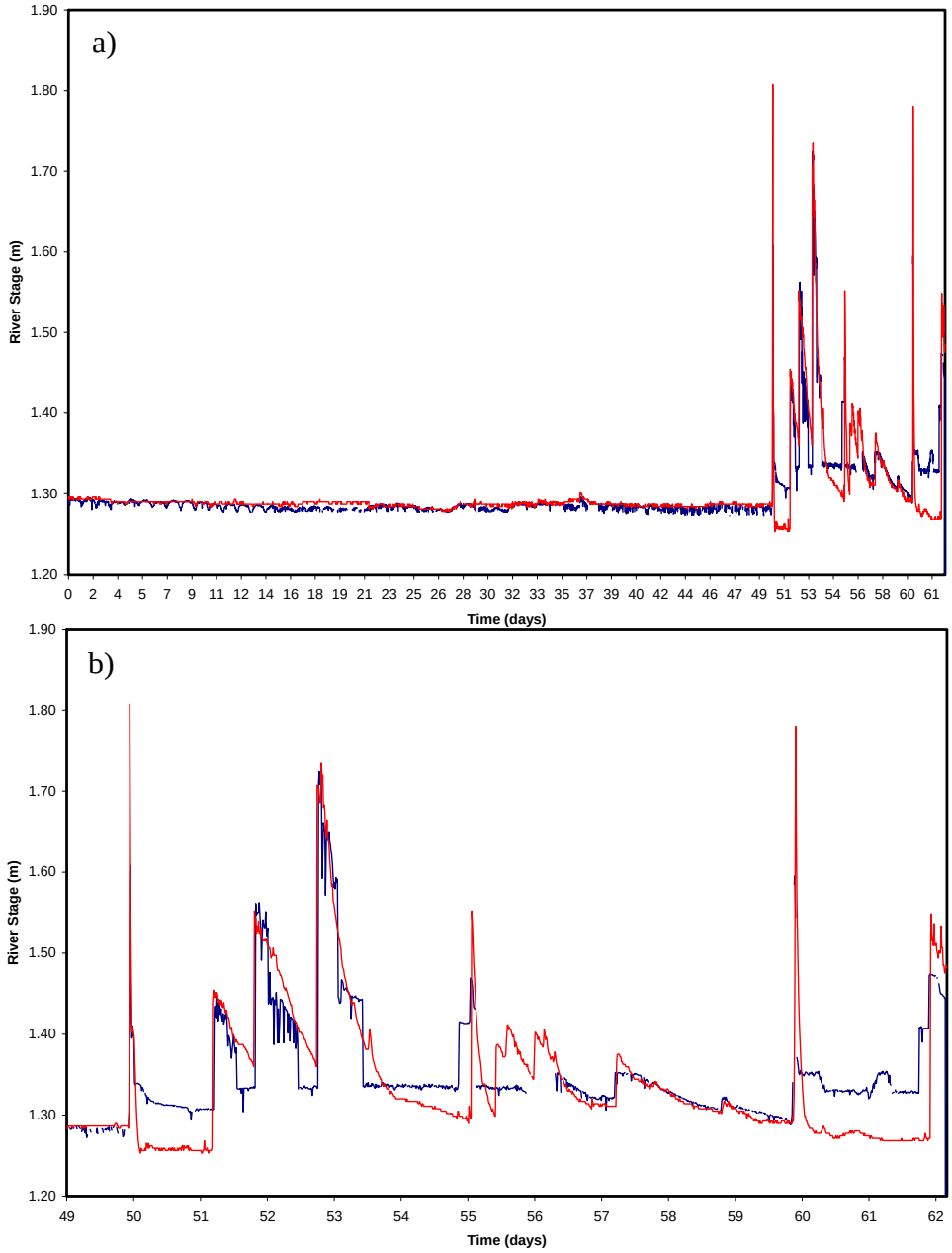

Figure 5.4: Comparison of stage measurements made on the Paria River with the TDR (blue line) and as measured by the USGS (red line). Data are for the period of a) May 25 to July 26, 2004, and b) July 13-26.

to decide which probe to sample than to the actual measurement by the TDR. Also, the TDR is seen to significantly overestimate stream stage during low water conditions encountered on days 50 to 56 and days 60 to 62. These discrepancies were the result of silt and sand burying the TDR probes as a result of the flash flows on days 50 and 60. Once buried, the probes were simply measuring the moisture of the sand and silt (except when flows overtopped the sand). The probes were dug out on day 56, thus returning them to normal operation until the next event.

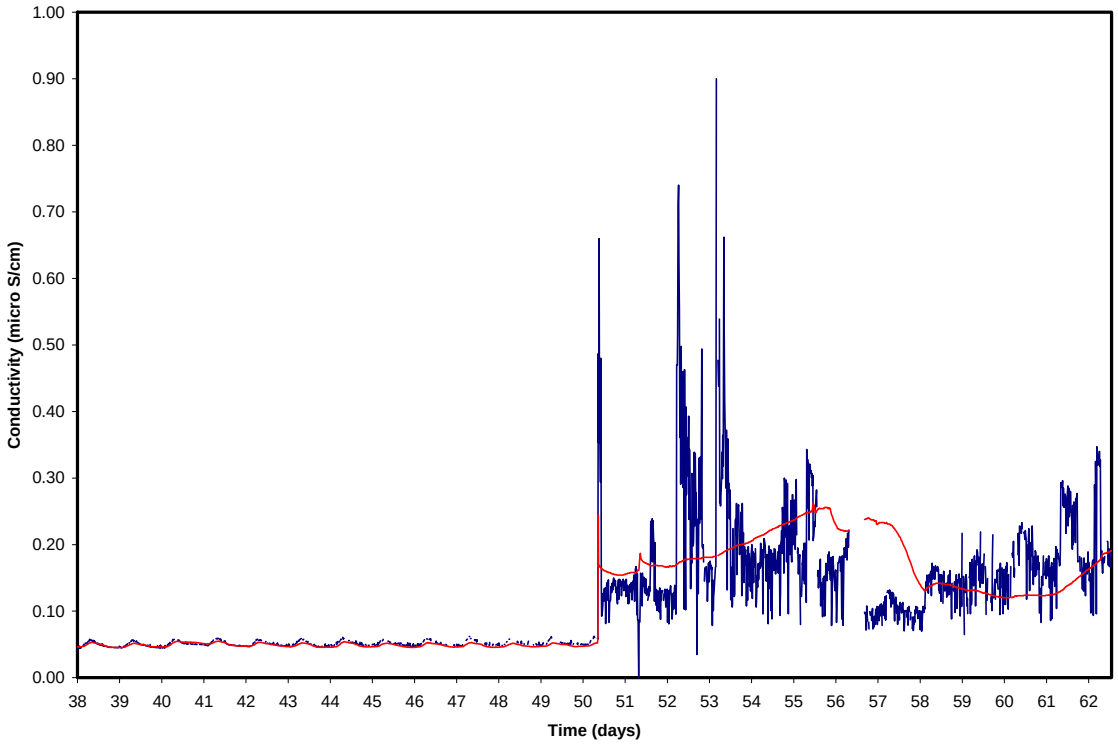

Figure 5.5: Comparison of aqueous conductivity measurements made on the Paria River with the TDR (blue line) and conductivity probe (red line). Data are for the period of July 2-25, 2004.

The Paria River proved to be a challenging environment for stream stage monitoring. This is reflected in increased error between the USGS and TDR measured steam stage data. For the entire 2-month period, the average deviation was ±1.76 cm. Much of this error could be alleviated by improving the data acquisition software and identifying/correcting the issue with the trace corruption. Difficulties with sand burying the probes following storm events is a problem for the TDR as well as most other technologies currently used to sense stream stage.

5.2.3. Aqueous conductivity measurements

Aqueous conductivity values were also estimated from the TDR traces acquired from the Paria River site. The measured conductivity from July 2-26, 2004 is plotted in Figure 5.5. Note that the conductivity probe was not functioning before this time, and thus the reason for the late start of the data. Conductivity values remain relatively constant for the first 50 days of monitoring. After day 50 conductivity values more than tripled, jumping from 0.048 μS/cm to over 0.90 μS/cm, following the flash storm event.

We again evaluate the accuracy of the TDR measured conductivity values by drawing comparisons with independently measured conductivity values acquired with a conductivity probe. Conductivity values were measured with a Campbell Scientific Conductivity Probe (see Table 4.1) co-located with the TDR probes. Measurements from the conductivity probe were

adjusted for temperature according to Equation 4.1, while TDR measurements required no adjustment as they showed no correlation to temperature.

Both the TDR and conductivity probe measured conductivities are shown in Figure 5.5. Both sets of data show a relatively constant conductivity for the first 50 days followed by a significant step increase during the day 50 flash flood. As with the stream stage data, good agreement between the TDR and conductivity probe is realized over the first 50 days. On average the two data sets differ by ± 0.002 μS/cm during this period. However, after day 50 significant differences in the two data sets are evident. Specifically, the TDR measured conductivities vary much more erratically than those values measured with the conductivity probe. One possible explanation for this behavior is the significant increase in sediment load conveyed by the Paria River due to the continuous string of high flow events. Alternatively, the conductivity probe was buried in sediment much of this time so it would not have been sufficiently sensitive to variations in aqueous conductivity. In conclusion, the measured error is believed to be a result of a combination of these two factors.

6. Summary

Here we explore application of Time Domain Reflectometry (TDR) to stream monitoring; specifically, the measurement of stream stage, channel profile and aqueous conductivity. These measurements take advantage of the impedance, reflection, and attenuation that the TDR signal experiences as it transverses a waveguide buried in a stream channel. Interest in this technology stems from the advantage of concurrently measuring stream stage and channel profile for improved monitoring of stream discharge, while at the same time providing continuous information on the conductivity.

Key to this application is a robust means of analyzing TDR data, providing good measurement accuracy under conditions involving the presence of multiple interfaces and/or multiple parameters varying simultaneously. The adopted analysis scheme employs the physically based multisection-modeling framework of the S_{11} scatter function and Cole-Cole parameters for dielectric dispersion and loss. Proof of concept experiments were performed to test and calibrate the model for application within a stream-monitoring context. These experiments employed acrylic tanks in which TDR probes were affixed. Experiments proceeded by making TDR measurements as the depth of water, depth of sand, conductivity, and length of coaxial cable were systematically varied. Multisection modeling [Heimovaara, 1994; Feng et al., 1999] was then used to interpret the acquired TDR traces. Results from a series of repeated tests suggest that the precision of the TDR in measuring the position of a water/sand interface is $\pm 3.6 \times 10^{-4}$ m while conductivity is measured with a precision of 1.95×10^{-4} μS/cm. Accuracy of the TDR measurements is $\pm 3.4 \times 10^{-3}$ m for sensing the location of an air/water or water/sediment interface and ±7.4% of actual for the conductivity. Additionally, the measured precision and accuracy were found to be independent of the location of the interface along the length of the probe and independent of the length of coaxial cable (up to 55 m) connecting the probe to the cable tester.

To explore the performance of the TDR under normal field conditions, TDR stream monitoring stations were established at two different locations. The first site was located on the Rio Grande at the Central Bridge in Albuquerque, NM. The site consisted of 8 probes, one designed to monitor stream stage and aqueous conductivity, while the other seven were anchored in the channel bed to monitor temporal changes in the channel profile. Operation of the site was initiated in March 2004 and has continued to collect data at hourly intervals to the time of this publication. To evaluate instrument accuracy, comparisons were drawn between the TDR measured data and other independently measured stream data. Comparison between TDR measured stream stage data and that measured by the USGS indicate that the two data sets were within ±0.88 cm over the 2-month analysis period. Comparisons between TDR measured conductivity and that measured with an ion specific probe yielded errors on the order of ±0.0046 μS/cm, which was roughly ±11% of the aqueous conductivity. Finally, channel profile measurements made with a hand staff were found to be within ±1.25 cm of that measured with

the TDR. In general, these results indicate strong potential for TDR as a stream monitoring technology

Another important result from the Rio Grande site was the measured channel profiles. These TDR measurements provided a continuous record of sand waves, dunes and bars moving across the anchored probes. To the knowledge of the authors, no similar measurements have ever been published. These results demonstrate the potential for TDR to track the movement of bedload features in an aqueous environment. More importantly, these time series could be used to develop quantitative estimates of the mobile bedload phase by simply integrating the area under the measured sand depth curves. By repeating this at several locations along a channel cross sections the mobile bedload for the entire river can easily be calculated.

The second field site was located on the Paria River near Lee's Ferry, AZ. At this site only stream stage and channel profile were measured. Operation of the site began on May 25, 2004 and was concluded on October 24, 2004. At this site, data were collected on 15-minute intervals. The monitoring environment at this site was considerably more difficult due to the occurrence of rapid flash flow events and heavy sediment loads accompanying these flows. As a result comparisons with independently measured data were not as good. Comparisons drawn with USGS measured stream stage data were within ±1.76 cm of that measured with the TDR, while conductivity values deviated by ±0.07μS/cm or ±30% of the measured conductivity relative to that measured with a conductivity probe.

In conclusion, time domain reflectometry proved to be a very able technology for stream monitoring. We found the TDR to be capable of measuring stream stage to better than ±1 cm and the conductivity to ±11% of actual (under field conditions). Although there are other techniques that might provide slightly better accuracy, TDR has the advantage that with one technology concurrent and continuous information on stream stage, aqueous conductivity and channel profile can be collected. Also unique to this methodology is the ability to track changes in channel elevation, or profile, continuously and in real time. Such information is critical in calculating stage-discharge rating curves and for estimating the active bedload being conveyed downstream by the river.

7. References

Clarkson, T.S., L. Glasser, R.W. Tuxworth, and G. Williams, An appreciation of experimental factors in time-domain spectroscopy, *Adv. Mol. Relax. Interact. Processes,* 10,173-202, 1977.

Dalton, F.N., W.N. Herkelrath, D.S. Rawlins, and J.D. Rhoades, Time domain reflectometry: Simultaneous measurement of soil water content and electrical conductivity with a single probe, *Science,* 224, 989-990, 1984.

Detlefsen, J., Frequency response of input impedance implies the distribution of discontinuities of a transmission line system, *Electron. Lett.*, 6, 67-69,1970.

Doherty, J., L. Brebber, and P. Whyte, *PEST2000 Model-Independent Parameter Estimation: User Manual*, Watermark Computing, 2000.

Dowding, C.H. and C.E. Pierce, Use of time domain reflectometry to detect bridge scour and monitor pier movement, *Proceeding of the Symposium and Workshop in Time Domain Reflectometry in Environmental Infrastructure and Mining Applications*, Northwestern University, Evanston, IL., 579-587, 1994.

Dowding, C.H., M.B. Su, and K.M. O'Connor, Measurement of rock mass deformation with grouted coaxial antenna cables, *Rock Mechanics and Rock Engineering*, 22, 1-23, 1989.

Feng, W., C.P. Lin, R.J. Deschamps, V.P. Drnevich, Theoretical model of a multisection time domain reflectometry measurement system, *Water Resour. Res.*, 35(8), 2321-2331, 1999.

Gorin, S.R. and F.P. Haeni, *Use of surface-geophysical methods to assess riverbed scour at bridge piers*, Water Resources Investigations Report No. 88-4212, U.S. Geological Survey, Hartford, Conn., 1989.

Gorski, G. and T. Anderson, Geotechnical assessment and monitoring: Buffalo-Ankerite Tailing Stack Timmins, Ontario, MMSL 98-021(TR), *Natural Resources Canada*, 31.p., 1998.

Hays, D.C. and F.E. Drummond, *Use of fathometers and electrical-conductivity probes to monitor riverbed scour at bridges and piers*, Water Resources Investigations Report No. 94-4164, U.S. Geological Survey, Hartford, Conn., 1995.

Hasted, J.B., *Aqueous Dielectrics*, Chapman and Hall, New Your, 1973.

Heimovaara, T.J., Frequency domain analysis of time domain reflectometry waveforms, 1. Measurement of the complex dielectric permittivity of soils, *Water Resour. Res.*, 30(2), 189-199, 1994.

Herkelrath W.N., S.P. Hamburg, F. Murphy, Automatic, real-time monitoring of soil moisture in a remote field area with time domain reflectometry, *Water Resour. Res.,* 27(5), 857-864, 1991.

Kane, W.F. and T.J. Beck, Raid slope monitoring, *Civil Engineering*, 666, 56-58, 1996.

Lagasse, P.F., E.V. Richardson, J.D. Shall, and G.R. Price, *Instrumentation measuring scour at bridge piers and abutments*, NCHRP Rep. 396, National Cooperative Highway Research Program, Washington, D.C., 1997.

Latkovitch, V.J. and G.H. Leavesley, Automated data acquisition and transmission, in *Handbook of Hydrology*, D.R. Maidment Ed., cp. 25, 1992.

Richardson, E.V. and P.F. Lagasse, *Instrumentation for measuring bridge scour at bridge piers and abutments*, Phase II Final Report, National Cooperative Highway Resources Program, Transportation Resources Board, National Research Council, Washington, D.C., 1994.

Topp, G.C., J.L. Davis and A.P. Annan, Electromagnetic determination of soil water content: Measurements in coaxial transmission lines, *Water Resour. Res.,* 16(3), 574-582, 1980.

Yankielun, N.E. and L.J. Zabilansky, Innovative instrumentation Techniques for Detecting and Measuring the Effects of Sediment Scour Under Ice. *Proceedings, ASCE Water Resources Engineering '98*, Memphis TN 3-7 Aug 1998 Vol. 1, 1998.

Yankielun, N.E., and L. Zabilansky, Laboratory investigation of time-domain reflectometry system for monitoring bridge scour, *Journal of Hydraulic Engineering*, 1279-1284, December 1999.

Zabilansky, L.J., *Ice force and scour instrumentation for the White River*, Vermont, CRREL Report. U.S. Army Corps of Engineers, Cold Regions Research and Engineering 1996.

Zabilansky, L.J., Ice cover effects on bed scour: Case studies. *Proceedings 11th ASCE Cold Regions Engineering*, Anchorage, Alaska, 19-23 May 2002.

Zabilansky, L., R. Ettema, J.L. Wuebben and N.E. Yankielun, *Survey of river-ice influences on channel bathymetry along the Fort Peck reach of the Missouri River, winter 1998-1999*. CRREL Report. U.S. Army Corps of Engineers, Cold Regions Research and Engineering, 2002.

Appendix: Alternative Waveguide Design

Field implementation of the TDR stream monitoring system provided the opportunity to identify shortcomings of the sensors. The most obvious sensor shortcoming is the limit imposed on waveguide length, which limits the measurement range of both water surface and streambed elevation. This limitation is imposed both by attenuation of the TDR signal due to electrical conductivity of the water and the need to secure sensors to minimize damage during extreme flood events and from vandalism. The obvious solution to these problems is to have a sensor with moveable waveguides and an automated control system for moving the waveguides as conditions warrant. As part of this research project, we investigated the feasibility of constructing such a system using off-the-shelf components to minimize cost. During this effort, and before the project funding was exhausted, we were able to formulate a design and locate most of the commercially available components that could be used in this system. The next step would have involved working out the engineering details of the actuator system and the design details required to assemble the components. A description of the proposed moveable waveguide sensor and a record of the components of the design are provided below.

Three waveguides are mounted on a moveable cylinder installed within a larger housing/cylinder (Figures A.1 and A.2). Actuation of the moveable cylinder relies on compressed air provided by a small air compressor and a solenoid operated valve located on the shore. Compressed air is delivered to the air/water chambers mounted on the sensor body, which then provides pressurized water to the driver piston and cylinder assembly attached to the moveable cylinder. An ultra high molecular weight polyethylene (UHMWP) seal designed for use in abrasive environments provides a seal between the moveable cylinder and the sensor housing. Two linear magnetostrictive sensors, one mounted on the top of the housing and the other on the bottom monitor the movement of the moveable cylinder and provide feedback to a control system that operates the solenoid valve to control the rate and magnitude of movement of the moveable cylinder. The compressed air drives the cylinder upward or downward 40 cm from a center position for a total travel of 80 cm. A light positive pressure is maintained inside the housing to prevent water leakage from volume changes during actuation. This pressure balance is accomplished with relief apertures, which eliminate the need for valves in the buried package. This entire package is buried beneath the silt water boundary with only the waveguides protruding up through the riverbed and into the water.

The compressed air delivery system is installed/buried on/in the riverbank in a secure enclosure. Compressed air is stored in sufficient volume to actuate an array of six probe assemblies in a 24-hour period. A solenoid valve is dedicated to each probe assembly. The storage tank is charged by a 12V compressor powered by batteries, which are charged with PV panels. The compressor can be left unattended for up to 1 year.

Descriptions and part numbers of the major components are given in Table A.2.

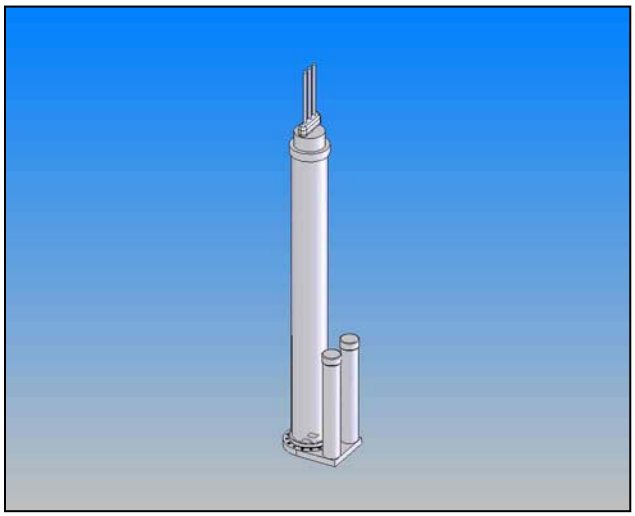

Figure A.1. Schematic showing the TDR moveable waveguide assembly.

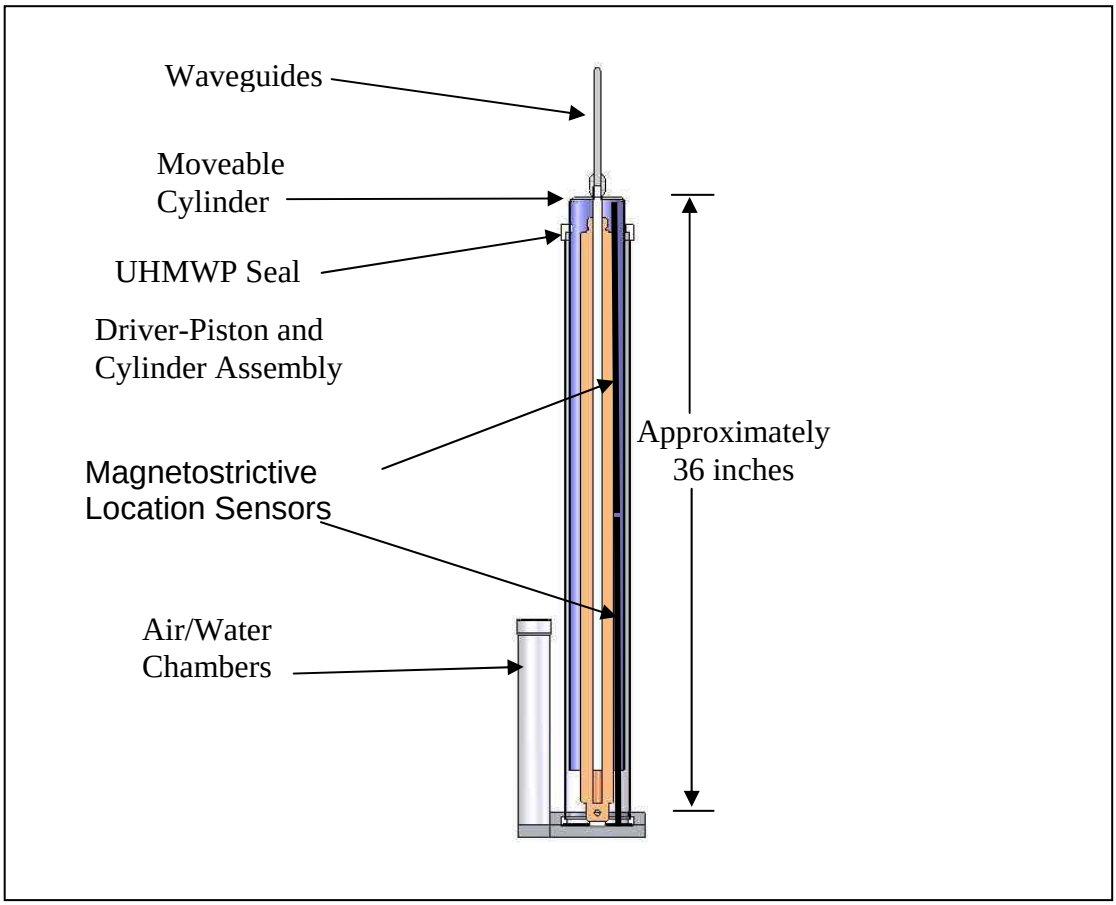

Figure A.2. Cross-sectional view of the major components of the TDR moveable waveguide as discussed in the text.

Table A.1. Description of a selection of the major components of the TDR moveable waveguide shown in Figure 2 and the air compressor (not shown)

Description	Manufacturer	Part Number/Type	Notes
Waveguides	Custom made	NA	3/16 diameter stainless steel rods
Moveable Cylinder	Custom made	NA	High density chrome cold drawn tube
UHMWP Seal:	Parker[1]	114UHMWPE	Ultra High Molecular Weight Polyethylene. High wearing plastic for use in abrasive water based medias
Driver Piston Assembly	Parker[1]	SRD/SRDM Mounting Style DXP	
Location Sensors	MTS[2]	CSP NH Style	Highly durable-non contact design
Air Compressor	Geotech[3]	12 volt DC compressor	

[1]Parker EPS Division – Chicago Operations
2565 Northwest Parkway
Elgin, IL 60123
(847) 783-4300

[2]MTS Systems Corporation
14000 Technology Drive
Eden Prairie, MN 55344-2290
Telephone: 952-937-4000

[3]GEOTECH Environmental Equipment, Inc
8035 East 40th Avenue
Denver, CO 8027
(303) 320-4764

Distribution

Internal

3	MS-0735	V. Tidwell, 6115
2	MS-0735	J. Wright, 6115
1	MS-0735	J. Brainard, 6115
1	MS-1395	J. Roberts, 6822
1	MS-1372	J. Coombs, 6926
1	MS-0703	D. Ruby, 6218
1	MS-1135	R. Jepsen, 9134
1	MS-0735	R. Finley, 6115
1	MS-0701	P. Davies, 6100
1	MS-0701	J. Merson, 6102
1	MS-0750	T. Hinkebein, 6118
1	MS-0708	M. Hightower, 6202
1	MS-0734	Wayne Einfeld, 6245
1	MS-0735	R. Pate, 6115
1	MS-1395	M. Rigali, 6822
1	MS-0123	D. Chavez, LDRD Office, 1011
1	MS-9018	Central Technical Files, 8945-1
2	MS-0899	Technical Library, 9616
1	MS-0612	Review & Approval Desk, 9612

External

1 Nancy Hornew
United States Geological Survey
Water Resources Division
2255 N. Gemini Drive
Flagstaff, AZ 86001

1 Mike Roark
United States Geological Survey
5338 Montgomery, NE
Suite 400
Albuquerque, NM 87109-1311